© 2013 Science Wise Publishing & DE GRUYTER DOI 10.1515/nanoph-2012-0031 — Nanophotonics 2013; 2(1): 57–81

Review article

Talha Erdem and Hilmi Volkan Demir*

Color science of nanocrystal quantum dots for lighting and displays

Abstract: Colloidal nanocrystals of semiconductor quantum dots (QDs) are gaining prominence among the optoelectronic materials in the photonics industry. Among their many applications, their use in artificial lighting and displays has attracted special attention thanks to their high efficiency and narrow emission band, enabling spectral purity and fine tunability. By employing QDs in color-conversion LEDs, it is possible to simultaneously accomplish successful color rendition of the illuminated objects together with a good spectral overlap between the emission spectrum of the device and the sensitivity of the human eye, in addition to a warm white color, in contrast to other conventional sources such as incandescent and fluorescent lamps, and phosphor-based LEDs, which cannot achieve all of these properties at the same time. In this review, we summarize the color science of QDs for lighting and displays, and present the recent developments in QD-integrated LEDs and display research. First, we start with a general introduction to color science, photometry, and radiometry. After presenting an overview of QDs, we continue with the spectral designs of QD-integrated white LEDs that have led to efficient lighting for indoor and outdoor applications. Subsequently, we discuss QD color-conversion LEDs and displays as proof-of-concept applications – a new paradigm in artificial lighting and displays. Finally, we conclude with a summary of research opportunities and challenges along with a future outlook.

Keywords: quantum dots; nanocrysrtals; light emitting diodes; color science; photometry; displays.

***Corresponding author: Hilmi Volkan Demir**, Institute of Materials Science and Nanotechnology, Departments of Electrical and Electronics Engineering, Physics, UNAM-National Nanotechnology Research Center, Bilkent, Ankara 06800, Turkey, e-mail: volkan@bilkent.edu.tr; hvdemir@ntu.edu.sg; and Luminous! Center of Excellence for Semiconductor Lighting and Displays, School of Electrical and Electronic Engineering, School of Physical and Mathematical Sciences, Nanyang Technological University, 639798, Singapore

Talha Erdem: Institute of Materials Science and Nanotechnology, Departments of Electrical and Electronics Engineering, Physics, UNAM-National Nanotechnology Research Center, Bilkent, Ankara 06800, Turkey

Edited by Romain Quidant

1 Introduction

In terms of saving energy, lighting has significant potential as artificial lighting constitutes approximately 20% of the global electrical energy consumption [1]; in some regions of the world, this amount even increases above 30% [2]. As a means of decreasing this number, solid-state lighting (SSL) offers great potential, with a projected reduction of 50% in the electricity consumption occurring due to lighting [3]. As the US Department of Energy reports, replacing all the existing light sources with light-emitting diodes (LEDs) will result in saving 133 TWh of electrical energy annually in the USA [4].

General lighting applications require white light, which is generated using sources like incandescent, fluorescent, high-pressure sodium lamps, mercury vapor lamps, and LEDs. Because of their energy-saving potential, LEDs have been attracting great of attention for a decade, both in the research community and in industry. Different techniques for generating a white light spectrum using LEDs have been proposed. One approach is the simultaneous use of multiple LED chips emitting different colors; however, important drawbacks of this method have prevented its widespread preference. First, no efficient material system suitable for green LED is currently available. In addition, using multiple chips at the same time requires complicated electrical circuitry, which increases the cost of the final LED lamp. Therefore, the desired efficiency and cost-effectiveness cannot be obtained using this approach. As an alternative method, white LEDs can be obtained by integrating color-converting materials on a blue- or near-UV-emitting LED chip. Today, most of the white LEDs are produced by employing rare-earth-ion-based phosphors as color-conversion materials. These materials exhibit high absorption at short wavelengths and a broad emission covering the whole visible spectrum. Significant progress has been made to improve their energy efficiency. Currently, other commercial light sources like fluorescent and incandescent lamps have already been surpassed in terms of energy efficiency. However, current phosphor-based white LEDs have limitations, especially on the

color quality and spectral efficiency. These LEDs cannot simultaneously accomplish a good color rendition, a good spectral match with the spectral sensitivity of the human eye, and a warm white shade, although individual high performances are possible. This basically emanates from the difficulties in the spectral tuning of phosphors. In addition, concerns regarding the supply of and current commercial monopoly on phosphors have increased the demand for alternative color converters [5]. At this point, quantum dots are rising as a promising candidate since they exhibit fine spectral tuning, achieved by their size control and narrow-band emission [6]. Therefore, with optimized spectral designs, the real colors of objects can be rendered properly while achieving a warm white shade and a good spectral overlap with the human eye sensitivity function, which in turn increases the efficiency of the light source; all of these improvements can be achieved at the same time with QDs employed in white LEDs [7, 8]. Furthermore, their high photoluminescence quantum efficiencies can contribute to realizing the high electrical efficiency of the device [9, 10]. Considering these features of QDs, they offer great potential for white LEDs by possessing high color quality along with photometric and electrical efficiency. In addition to general lighting applications, QD-based LEDs can easily respond to the demands of the backlights used in liquid crystal displays (LCD). In particular, the narrow emission band of QDs enables the reproduction of high purity colors. Moreover, a much larger number of colors can be generated using these materials; in other words, the color gamut of the LCDs can be broadened beyond the industrial standards.

At this point it is useful to distinguish two types of LEDs using QDs, which rely on two different means of excitation. One is based on electrically exciting the QDs, which makes LEDs based on the direct electroluminescence of QDs, and the other is through optically exciting them, which makes color-conversion LEDs using QDs as the nanophosphors. As the name implies, in the electrically excited QD based LEDs, electrons and holes are directly injected into the quantum dots, and the white light emission is thus obtained through the radiative recombination of these injected carriers within QDs having different sizes and emitting different colors. Over the years to date, the overall efficiencies of these LEDs typically remained lower compared to those of color converting QD-WLEDs mainly because of the charge injection problem. The organic ligands surrounding the QDs, whose main function is the passivation of the QD surface, are poor conductive materials and generate a large barrier that makes the charge injection difficult. Therefore, the injection of carriers into the QDs is not an easy task which in the end decreases the overall device efficiency. Despite this challenge, significant improvements have been realized within the past decade. Another difficulty arises from the issues related to charge accumulation and photocharging effects for operation over a long time. For further information on this topic, we recommend the excellent reviews written by Rogach et al. [11] and Wood and Bulović [12]. Here, we focus on the QD-WLEDs based on color conversion using QD photoluminescence rather than QD electroluminescence. Since there is no carrier injection into QDs in these devices, they do not suffer from the problems of the electrically excited ones. Although there is some energy loss due to the conversion of highly energetic photons (usually blue or UV) to low energy photons to generate white light (Stokes' shift), the energy penalty is not as severe as the efficiency reduction due to charge injection in the case of electrically excited QD-based LEDs. It is also worth mentioning here that, although realizing color conversion using this method can be simple, generating high quality white light suitable for general lighting applications requires very careful colorimetric and photometric optimizations which depend on a deeper understanding of the color science and photometry.

In order to obtain the desired performance, scientists and researchers all around the world have carried out studies, both experimentally and theoretically, resulting in significant improvements in the area. In this review, we summarize these developments on general lighting and display backlighting where QDs replace the conventional color-converting phosphors. Before covering the reported studies, we first start with a general overview of color science and photometry, which basically introduces the figure-of-merits for general lighting applications. Subsequently, we review the research on the spectral design of QD-integrated white LEDs (QD-WLEDs) for indoor and outdoor lighting applications. Then we continue with a summary of the experimental demonstrations of QD-WLEDs. The subsequent section is devoted to the application of QDs as LCD backlights. Finally, we conclude the review by discussing the future outlook and challenges for QDs and their LEDs.

2 The human eye, color science, and photometry

To evaluate the quality of white light sources, one needs to have quantitative measures, some of which also take human perception into account. At this point, color science and photometry along with radiometry comes into play. In this section, we summarize these concepts by first explaining the main features of the human eye. Subsequently,

we discuss the color rendition metrics that indicate how accurate the real colors of the objects are rendered by the light source. Following this, we move to the photometry and discuss the different vision regimes depending on the luminance levels. We discuss the changes in the sensitivity of the human eye, followed by the figure-of-merits considering the spectral match between the light source and the sensitivity of the human eye.

2.1 The structure of the human eye

The eye is the sensory organ that provides us with the faculty of visual perception. Therefore, knowing its structure is very helpful for understanding the vision process. The outermost layer of the eye is called the cornea, where the light rays first enter (Figure 1). There is an additional curvature in the front part of the cornea. The cornea itself is a transparent structure; moreover, tears and mucus solutions have an important role in sustaining the transparency of the cornea. Light rays passing through the cornea arrive at the so-called anterior chamber, which is full of a transparent liquid known as the aqueous humor that controls the pressure within the eyeball. After traversing this liquid region, light rays come to the lens which is responsible for focusing the incoming rays on the retina [13].

The retina is the part of the eye where the photoreceptors, neurons, and fibers are located. According to Stell, the visual neurons consist of three main layers [15]. The first layer is the layer of photoreceptors; the second one is the layer of intermediate neurons. Finally, the third neural layer is the layer of ganglion cells. The light-sensitive cells are called photoreceptors. There are two types of them responsible for vision: rods and cones, named in accordance with their shapes. The retina is rich in rods, which are more sensitive to light than cones. Their sensitivity covers the whole visible range without useful color differentiation; as a result, they cannot deliver color information to the brain. On the other hand; cones have three types, each having a different wavelength range of sensitivity corresponding to blue, green, and red colors (Figure 2) [16]. In addition to their spectral sensitivities, their activity differs depending on the ambient lighting levels. At high luminances, cones are more active, and they are primarily responsible for vision, whereas rods do not have any significant contribution to the vision. This vision at high light levels is called photopic vision. On the other hand, cones are not sensitive enough at lower luminances, while rods are primarily responsible for vision. This is why we cannot distinguish different colors in the dark. This vision regime is called scotopic. There is another vision regime where rods and cones are both active and contribute to the vision simultaneously. This regime is called mesopic vision, the limits and significance of which will be discussed in the upcoming sections.

2.2 Color matching functions and color spaces

To engineer light sources, one needs to define colors from a mathematical perspective. Using a statistical approach, the International Commission for Illumination (Commission Internationale de l'Eclairage, CIE) utilized three color matching functions: x, y and z, whose spectral distributions are given in Figure 3 [17].

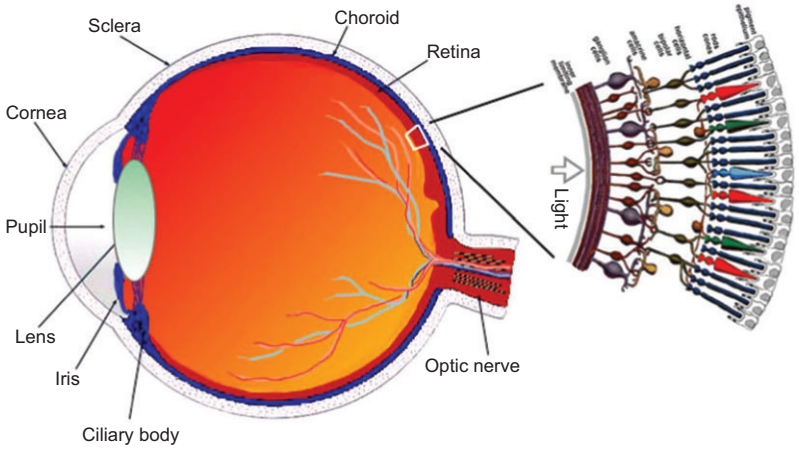

Figure 1 A cross-section of the human eye and a magnified view at the retina [14].

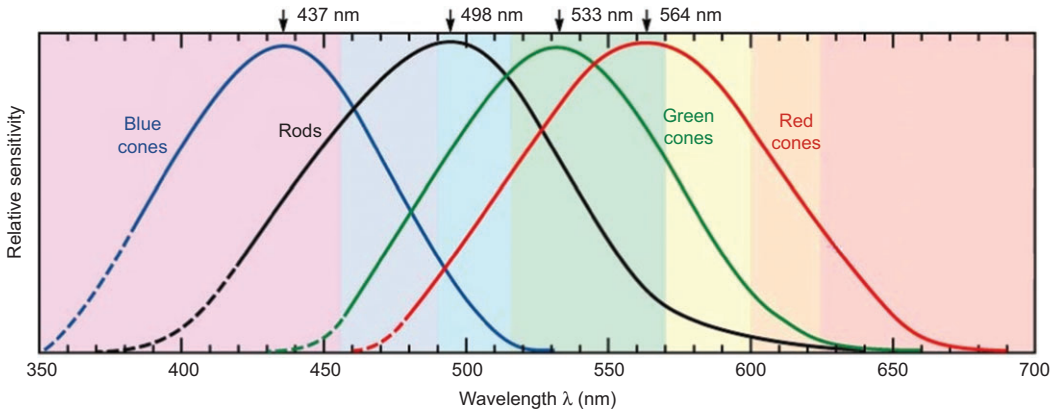

Figure 2 Normalized spectral sensitivities of rods and cones (red, green, and blue) [16].

The method proposed by the CIE makes use of these color matching functions and the chromaticity diagram. The tristimulus values, X, Y and Z, are given in Equations (1)–(3) for a spectral power distribution of $s(\lambda)$.

$$X=\int_{\lambda} s(\lambda)\bar{x}(\lambda)d\lambda \tag{1}$$

$$Y=\int_{\lambda} s(\lambda)\bar{y}(\lambda)d\lambda \tag{2}$$

$$Z=\int_{\lambda} s(\lambda)\bar{z}(\lambda)d\lambda \tag{3}$$

The chromaticity coordinates are calculated as in Equations (4)–(6). The chromaticity diagram, which is created by using the mapping methodology described in Equations (1)–(6), is given in Figure 4. Since one of the three coordinates is dependent on the other two, a two-dimensional color space is sufficient without any information loss. Therefore, Figure 4 is a two-dimensional diagram.

$$x=\frac{X}{X+Y+Z} \tag{4}$$

$$y=\frac{Y}{X+Y+Z} \tag{5}$$

$$z=\frac{Z}{X+Y+Z}=1-x-y \tag{6}$$

Although CIE 1931 is the most widely used chromaticity diagram, it has some important weaknesses, which were later improved by defining new color spaces. One of the important drawbacks of CIE 1931 is that the geometric difference between the positions of pairs of colors in this diagram does not consistently correspond to the perceived difference between the colors. To fix this problem, the CIE introduced new chromaticity diagrams in 1960 and 1976. These diagrams are called the (u, v), (u', v'), and $L^*a^*b^*$

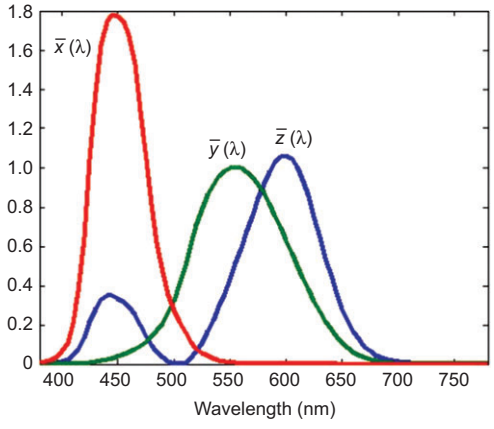

Figure 3 Color matching functions as defined in CIE 1931 [17].

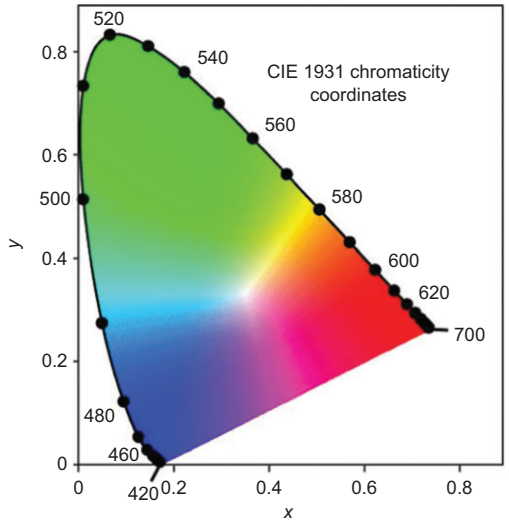

Figure 4 CIE 1931 (x, y) chromaticity diagram [18].

chromaticity diagrams; further information regarding these color spaces can be found in Ref. [19].

2.3 Color rendering index and color quality scale

A good white light source must render the real colors of the objects that it illuminates. This feature of light sources has great importance for indoor lighting applications (Figure 5). Moreover, under low ambient lighting such as outdoor lighting, Reynham and Saksvrikrønning indicated that good color rendition helps increase road safety by improving the color contrast [20].

The color rendering capability of the illuminants is evaluated by several methods. In this section, we will briefly mention two metrics that are used very frequently. These are the color rendering index (CRI) developed by the CIE and the color quality scale (CQS), which was developed by Davis and Ohno at the National Institute of Standards and Technology (NIST) [21]. Other than these two, there are several different metrics such as the color discrimination index [22], cone surface area [23], color rendering capacity [24], feeling of contrast index [25], and flattery index [26]. These metrics have not been as widely used in the lighting community to date; therefore, we will not cover them here in detail.

The color rendering index was developed by the CIE in 1971 [27] and updated to its current form in 1995 [28]. It basically tests the color rendering capability of the test light source with respect to a reference light source, which is assumed to possess perfect color rendition. The CRI makes use of 14 test color samples suggested by the CIE. Based on the reflection of the test light source and the reference light source from these samples, color differences are calculated for each test sample. Finally, from these color differences, a color rendering index value specific for each sample is obtained. The first eight of these samples are used for determining the general color rendering index. The remaining six define the special color rendering indices. The best color rendition is given as 100, whereas the worst rendition is denoted by a CRI of -100.

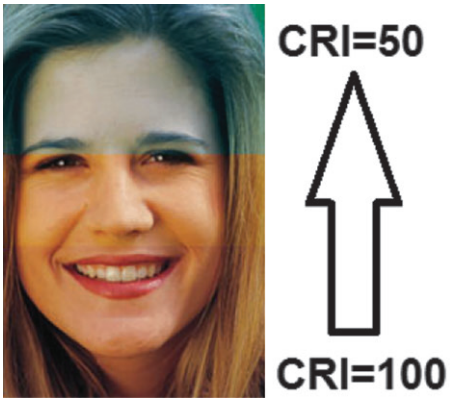

Figure 5 Photograph of a woman face illuminated with different sources having different CRIs [30].

Although the CRI is still the most frequently used metric for color rendition, it suffers from some weaknesses that need to be overcome [21]. One of these problems is the uniform color space used in the CRI, which is not recommended by the CIE any longer since the calculated color differences may not be accurate enough. Another important issue regarding the CRI is that it assumes perfect color rendering of blackbody radiators and reference sources, even at very low and high correlated color temperatures (CCTs, which will be explained in the next section). However, this is not always correct. Furthermore, the CRI does not use any test color sample that is highly saturated. As a result, it does not provide correct color rendering information of saturated colors, although the results are accurate for samples having desaturated colors. Furthermore, the CRI makes use of the arithmetic mean of color rendering indices of each test color sample, which means that a poor rendering for one of the samples can be compensated by the successful rendering of other test samples.

Considering these problems with the CRI, Davis and Ohno developed a new metric, the so-called color quality scale, for color rendering evaluation of light sources [21]. It uses the same reference light sources as in the CRI, but the test color samples are changed. Instead of eight unsaturated test color samples, CQS employs 15 commercially available Munsell samples, all having highly saturated colors. Since a light source that renders the saturated colors well succeeds in delivering a good rendition of unsaturated colors, this metric provides superior color rendering information. This is especially useful for narrow-band emitters such as light-emitting diodes and quantum dots. As it is done in the calculation of the CRI, a chromatic adaptation transform is necessary in the CQS, which utilizes a modern transform, CMCCAT2000 [29]. Another important improvement of the CQS compared to the CRI is the choice of a uniform color space. In the CQS, the CIE $L^*a^*b^*$ is preferred. In addition to the color difference, a saturation factor is introduced in the CQS so that the effect of increasing the object chroma under the test illuminant with respect to a reference source is neutralized. One of the most important improvements of the CQS compared to the CRI is

in the calculation of the final color rendering performance. In contrast with the CRI, the CQS calculates the root-mean-square values (rms) of individual corrected color differences, so that poor rendition of any test color sample has a more significant effect on the final value. An additional difference of the CQS as compared to the CRI is its scale. Since having a CRI less than zero, which denotes a poor color rendition, can be misleading, the CQS is transformed to a scale of 0–100. As in the case of the CRI, the best color rendition is denoted by 100 in the CQS, but in this case, the worst color rendition is expressed by 0. Finally, a correction for the low CCTs is introduced, and the final value of the CQS is determined.

2.4 Correlated color temperature

The shade of a white light source is expressed using the correlated color temperature (CCT). Before defining the CCT, it is necessary first to explain the color temperature. If the chromaticity coordinates of the white light source fall onto the Planckian locus (chromaticity coordinates of blackbody radiators at different temperatures), then the temperature of the blackbody radiator having the same chromaticity points as the white light source is called the color temperature (Figure 6). In the case that the chromaticity coordinates of the light source being tested are not on the Planckian locus, then the temperature of the blackbody radiator, whose (u', v') chromaticity coordinates are closest to the light source being tested, is defined to be the correlated color temperature.

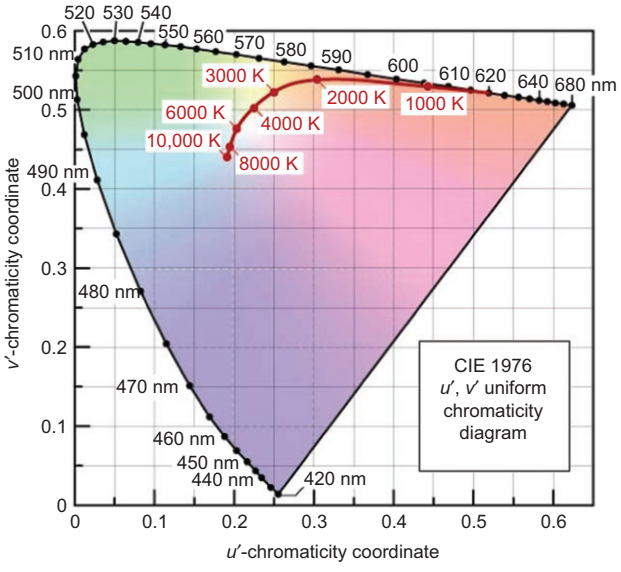

Figure 6 Planckian locus on CIE 1976 (u', v') chromaticity diagram [16].

White light sources having high CCTs have a bluish shade, whereas a reddish shade corresponds to lower CCTs. Therefore, cold (or cool) white light has a higher CCT and warm white sources have lower CCTs, which might look confusing at first sight since the use of the terminology is opposite to the common color codings for temperature. Incandescent light bulbs have CCTs around 3000 K and fluorescent tubes have varying CCTs from 3000 to 6500 K, whereas the CCT of the sun is close to 6000 K [16]. Having a warmer white shade (between 3000 and 4500 K) is more desirable for indoor lighting applications mainly because of the disturbing effects of cool white light on the human circadian cycle aka biological clock.

2.5 Eye sensitivity functions, radiometry, and photometry

While evaluating the quality of white light sources, it is of significant importance that the spectra of the illuminants match the sensitivity of the human eye as well as possible. This is because a light source radiating at wavelengths not detectable by the eye cannot contribute to what one sees. Even if it has a high power conversion efficiency or high optical power, this source cannot be accepted as an efficient light source for general lighting applications since the emitted light cannot be sensed. Therefore, light sources should be designed such that the optical energy spectrum overlaps with the human eye sensitivity spectrum as much as possible. At this point, knowing the sensitivities of the photoreceptors in the human eye is of critical importance. Since the photoreceptors contributing to vision are different at different ambient light levels, the sensitivity of the eye changes accordingly. Rod photoreceptors are responsible for scotopic vision, which is the dark-adapted vision [16]. Its sensitivity has a maximum at 507 nm. On the other hand, cones provide light-adapted vision and start to work above some luminance level. The vision at these light levels is then photopic. The sensitivity of the cones peaks at 555 nm. The vision regime where the lighting level is between the photopic and scotopic regimes, so that cones and rods both contribute to vision, is called the mesopic vision. The corresponding eye sensitivity functions for scotopic [31] and photopic [17] light levels are given in Figure 7 along with the sensitivity function of the mesopic regime for a photopic luminance of 0.5 cd/m^2.

While explaining the vision regimes, it is necessary to define some radiometric and photometric quantities.

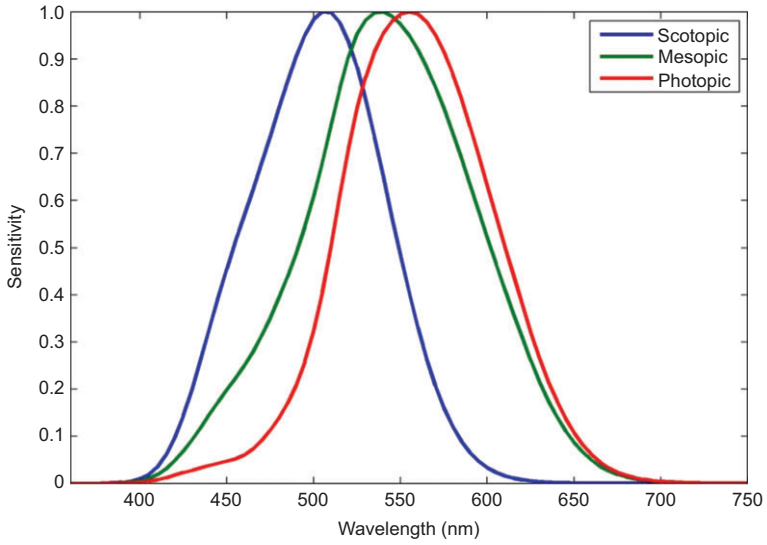

Figure 7 Eye sensitivity function in different vision regimes: photopic (red), mesopic (green, at a luminance of 0.5 cd/m^2), and scotopic eye sensitivity functions.

The radiometric measures express the properties of the light from the perspective of electromagnetic radiation. On the other hand, photometric measures evaluate the emitted spectrum considering the sensitivity of the human eye, and they are essential for commenting on the efficiency of white light sources for general lighting applications.

One of the most important pairs of radiometric-photometric quantities is radiance and luminance. The radiance is the radiometric quantity denoting the optical power per solid angle per unit area and has the units of $W_{opt}/(m^2sr)$. Given the spectral radiance $P_L(\lambda)$, the luminance is calculated using Equation (7). Basically, it gives us the amount of optical radiance that is useful for the human eye using the sensitivity function in the photopic regime $V(\lambda)$. It is measured in units of lm/(m^{2}sr), or equivalently cd/m^2.

$$L=683\frac{lm}{W_{opt}}\int P_L(\lambda)V(\lambda)d\lambda \tag{7}$$

The luminance levels are used for defining the vision regime boundaries. Previously, there has been no consensus regarding these limits until 2010. For example, Osram Sylvania reported the luminance limits of photopic and scotopic vision to be 0.003 and 3 cd/m^2, respectively [32] whereas Johnson [33] and LeGrand [34] stated that photopic vision begins at a luminance of 5 cd/m^2. According to Kokoschka, photopic vision starts at 10 cd/m^2 [35]. Moreover, the Illuminating Engineering Society of North America (IESNA) puts the boundaries at 0.01 and 3 cd/m^2 [36], and in 1978, the CIE reported that scotopic vision starts below 0.001 cd/m^2 [37]. Recently, Rea put the scotopic and photopic boundaries at 0.001 cd/m^2 and 0.6 cd/m^2, respectively [38]. Almost simultaneously, the MOVE consortium suggested the boundaries to be 0.01 cd/m^2 and 10 cd/m^2 [39, 40]. In 2010, a new report on a recommended system of photometry (CIE 191:2010) was published by the CIE, based on the USP and MOVE systems [41]. In this system, the boundary between the scotopic and mesopic vision was given as 0.005 cd/m^2 and that between the mesopic and photopic vision, as 5 cd/m^2. In this report, the eye sensitivity function, which indicates the responses of both rods and cones, was also defined, along with a mesopic luminance. These functions are calculated using Equations (8) and (9), respectively.

$$M(m)V_{mes}(\lambda)=mV(\lambda)+(1-m)V'(\lambda) \tag{8}$$

$$L_{mes}=683/V_{mes}(\lambda_0)\int V_{mes}(\lambda)P(\lambda)d\lambda \tag{9}$$

In the equations given above $V(\lambda)$, $V'(\lambda)$, and $V_{mes}(\lambda)$ are the photopic, scotopic, and mesopic eye sensitivity functions, respectively; $P(\lambda)$ is the spectral radiance, $M(m)$ is a normalization constant equating the maximum value of $V_{mes}(\lambda)$ to 1, and λ_0 is 555 nm. The mesopic luminance is represented by L_{mes}, and m is a coefficient that depends on the visual adaptation conditions. The details of this calculation can be found in Ref. [41].

Another radiometric quantity that needs to be known is the irradiance, which is the optical power per unit area. The unit of irradiance is W_{opt}/m^2. Similar to the case of the

luminance, the illuminance is the irradiance subject to the human eye sensitivity function, and it has units of lm/m^2 or equivalently lux. Given the spectral irradiance $P_I(\lambda)$, the illuminance is expressed as in Equation (10).

$$L_I = 683\frac{lm}{W_{opt}}\int P_I(\lambda)V(\lambda)\,d\lambda \tag{10}$$

The illuminance is used for investigating the effect of illumination on the human circadian cycle. Recent studies have revealed that there is another receptor in the human eye, which is not responsible for vision but is instead responsible for the regulation of the circadian cycle, i.e., the daily biological rhythm [42, 43]. This receptor is called melanopsin, and it controls the circadian rhythm by secreting melatonin. During the daytime, melatonin secretion is suppressed and a daytime signal is sent to the brain. During the nighttime, melatonin is secreted and a nighttime signal is delivered to the brain. According to Rea, melatonin suppression is affected collectively by rods, cones, and melanopsin [42], while Gall employs a simpler method [43]. Today, there is not enough data to falsify either of these models [44].

At this point, it is worth parenthetically noting and discussing the effects of light on the circadian cycle. Since during the daytime, the sun radiates with a significant short-wavelength content compared to the radiation in the evening, it is expected that melatonin suppression is regulated mostly by the blue content of the spectrum. This is also verified by the models cited above. Moreover, insufficient exposure to bluish light in the morning was found to result in a shift in the circadian cycle [45]. Another important point is that the shade of the white light emission affects the circadian cycle. In the case of cool white illumination, the brain receives signals indicating that it is daytime because of melatonin suppression due to the strong blue content, whereas a warm white illumination does not cause shifts in the circadian cycle. In other words, the circadian cycle can be manipulated by adjusting the spectrum of the light source and its color temperature. Therefore, for home lighting applications, warm white colors should be selected to avoid the unintended effects of lighting on the circadian rhythm.

In addition to the measures explained above, the efficiency of the white light sources needs to be evaluated by taking the eye sensitivity function into account. There are two important efficient measures that are used for this purpose. The first one expresses the efficiency of the white light spectrum; this measure is called the luminous efficacy of optical radiation (LER). It is calculated with Equation (11) where $P(\lambda)$ and $V(\lambda)$ are the spectral power distribution and photopic eye sensitivity function, respectively. The LER is in units of lm/W$_{opt}$. The maximum value of the LER is 683 lm/W$_{opt}$; however, this can only be achieved with a monochromatic light source at 555 nm. A white light spectrum having an LER as high as possible is desirable, as it means less optical energy is radiated at the wavelengths where the eye is not sensitive.

$$LER = \frac{683\frac{lm}{W_{opt}}\int P(\lambda)V(\lambda)d\lambda}{\int P(\lambda)d\lambda} \tag{11}$$

The second important efficiency measure calculates the efficiency of the radiated light as perceived by the human eye with respect to the supplied electrical power, P_{elect}. This performance criterion of light sources is called the luminous efficiency (LE). It is expressed in units of lm/W$_{elect}$ and is calculated as given in Equation (12). Here it is instructive to point out that the LE is related to the LER through the power conversion efficiency (PCE). The relation is given by Equation (13).

$$LE = \frac{683\frac{lm}{W_{opt}}\int P(\lambda)V(\lambda)d\lambda}{P_{elect}} \tag{12}$$

$$LE = LER \times \frac{\int P(\lambda)d\lambda}{P_{elect}} = LER \times PCE \tag{13}$$

There is another figure-of-merit, which may be used as an indicator of the rod activity. This metric calculates the ratio of the scotopic LER to the photopic LER [see Equation (14)], and it is referred to as the scotopic/photopic (S/P) ratio of the source. According to Berman, a light source possessing a higher S/P ratio yields better perception of brightness together with a better visual acuity [46]. Moreover, Berman explains that a light source having a higher CCT causes smaller pupil openings, and therefore, incoming light rays are collected more in the central region of the retina, enhancing visual acuity [47].

$$S/P = \frac{1699\frac{lm}{W_{opt}}\int P(\lambda)V'(\lambda)d\lambda}{683\frac{lm}{W_{opt}}\int P(\lambda)V(\lambda)d\lambda} \tag{14}$$

Up to here, we have covered the main concepts of color science and photometry, which are frequently used in designing white light sources. The most widely figure-of-merits in color science and photometry are also further

Table 1 Common figure-of-merits used for white light sources.

Figure of merit	Color rendering index (CRI)	Color quality scale (CQS)	Correlated color temperature (CCT)	Luminous efficacy of optical radiation (LER)	Luminous efficiency (LE) (aka luminous efficacy)	Scotopic/ ohotopic of the source (S/P ratio)	Luminance (L)	Mesopic luminance (L_{mes})
Unit	**None**	**None**	**K**	**lm/W_{opt}**	**lm/W_{elect}**	**None**	**cd/m^2**	**cd_{mes}/m^2**
Short description	Indicates how good the real colors of the illuminated objects are rendered by the light source		Indicates the shade of the white light source – warm or cool white	Indicates the overlap between the human eye sensitivity curve and the light source spectral power density per generated optical power	Indicates the overlap between the human eye sensitivity curve and the light source spectral power density per supplied electrical power	Indicates the ratio of the brightness perception under scotopic and photopic vision regimes	Indicates the overlap between the human eye sensitivity and the light source spectrum – can be considered as perceived brightness under photopic vision conditions	Indicates the spectral overlap between the human eye sensitivity and the light source spectrum – can be considered as perceived brightness under mesopic vision conditions

summarized in Table 1 and a short description for each figure-of-merit along with their units is provided to assist the reader to follow the rest of the review, especially Sections 4 and 5.

3 Color-converting nanocrystal quantum dots

In recent decades, optoelectronic devices, which are based on semiconductor materials, have revolutionized our lifestyles. As new studies concentrate on manipulations of the materials at the nanometer scale, new structures employing quantum mechanical effects have begun to be developed. Colloidal semiconductor nanocrystal quantum dots (QDs) are one of these structures. Since the effective bandgap of these QDs can be tuned within or near the visible spectral range essentially using one material system, semiconductor QDs have an important place in photonics. Additionally, the optical characteristics of these materials can be controlled again by adjusting their size and size distribution. As a result, new types of lasers, light-emitting diodes, solar cells, and other new optoelectronic devices can be developed. From the perspective of white LEDs, these materials offer great potential as they enable optimization of the photometric and colorimetric properties of the device, because of the narrow emission band of QDs together with the positioning of the peak emission wavelength within the visual spectra band. This further provides the ability to accommodate multiple QD emitters finely tuned one by one to collectively generate the targeted spectrum. Also, the broadband absorption of QDs remove the constraint for the excitation wavelength as long as it is sufficiently below the band edge, whereas this is one of the main concerns for conventional phosphors with narrow absorption bands. In this section of this review, we will discuss the physical and chemical properties of these materials, mainly from the perspective of light-emitting diodes.

As the size of the materials is made smaller and smaller, classical mechanics becomes no longer sufficient to explain the material properties; instead, the governing mechanisms rely on the principles of quantum physics. For semiconductor nanocrystal QDs, the same physical principles are valid. In a semiconductor QD, the electrons and holes are confined in three dimensions, typically within a range of 2–10 nm [48]. This distance is also the typical extension of electrons and holes in a semiconductor material. Therefore, the electrons and holes inside the crystalline semiconductor start to feel the free space or any other surrounding material having a larger bandgap as a barrier. As a result, the system reduces to a finite quantum well problem, and discrete energy levels dictate the material properties. A

schematic illustration of a quantum dot is given below in Figure 8 along with the corresponding energy band diagram.

The emission and absorption spectra of the QDs reveal the quantum confinement effects on the nanometer-sized semiconductor crystals very clearly. First, a significant blue shift is observed in the emission spectrum of the semiconductor material compared to the bulk case. For example, a bulk CdSe crystal has an emission peak of 713 nm, whereas its quantum dots can emit at around 500 nm. Another interesting feature of the QDs is that this blue shift is strongly dependent on the size of the material. As the size of the QD decreases, the emission peak moves to higher energies corresponding to shorter wavelengths as a result of the narrowing well width. On the other hand, the bandwidth of the emission spectrum is strongly dependent of the size distribution of the QDs and the density of the trap states. As with the emission, the absorption features also exhibit a size-dependent behavior. As the size of the QD decreases, the absorption starts at higher photon energies or equivalently shorter wavelengths. Typical emission and absorption spectra of the QDs are given in Figure 9.

One of the most interesting types of QDs is the colloidal semiconductor QDs prepared via wet chemical techniques in a relatively cheap way. The required potential barrier is created by the surrounding medium, which in general consists of the organic molecules called ligands. The quantum confinement effects that depend on the size of the QD are controlled by adjusting the temperature, growth time, and reactants. Another common method for preparing QDs, which are different than the colloidal quantum dots focused on in this review, is the use of epitaxial growth techniques. In this method, the island of an energetically narrow bandgap material is surrounded by a matrix with a wider energy bandgap. However, in contrast to their colloidal counterparts, their epitaxy over large areas is not possible. Moreover, they require a substrate; therefore, their deposition on the LED chips as color converters is a challenge.

Colloidal nanocrystal QDs can be synthesized and dispersed in polar solvents, like water, as well as in non-polar solvents such as hexane, toluene, and chloroform. A good review of the synthesis of these materials can be found in Ref. [50], and two important recent studies can be found in Refs. [51, 52]. There are several possible materials that can be used for QD synthesis. Among them, CdS, CdSe, CdTe, ZnS, ZnSe, ZnTe, HgTe, PbSe, PbS, and InP can be given as common examples. However, using only the core generally does not result in a high photoluminescence quantum efficiency, which is defined as the emitted number of photons per absorbed photon. To enhance the emission capabilities of the QDs, a core/shell material system is preferred. In this system, an additional material having a higher bandgap surrounds the core. A careful choice of material decreases the lattice mismatch, leading to increased quantum efficiency [53]; as a result, more efficient QDs can be synthesized. Today, efficiencies of more than 90% have been reported using colloidal approach [9]. Typical material choices are CdSe/CdS, CdSe/CdS/ZnS, CdSe/ZnS, PbSe/PbS, CdTe/CdSe, CdSe/ZnTe, and InP/ZnS. Another material system that has attracted attention in recent years is doped quantum dots. These QDs consist of a semiconductor core doped with a transition metal. The absorbing material is the semiconductor, while the emission occurs through the dopants. As a result, the emission spectrum of the QDs and their absorption spectrum are very strongly separated, which in turn decreases the reabsorption problem [54]. Common core-QDs are InP, CdS, and ZnSe, and common transition metals acting as the dopant are Cu and Mn.

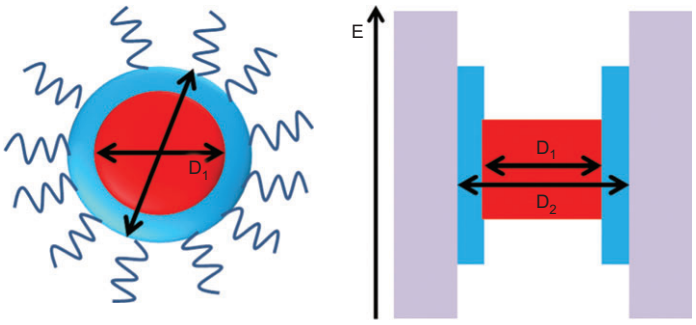

Figure 8 Semiconductor QDs: a schematic illustration of a core/shell semiconductor QD (left) and the associated band diagram (right).

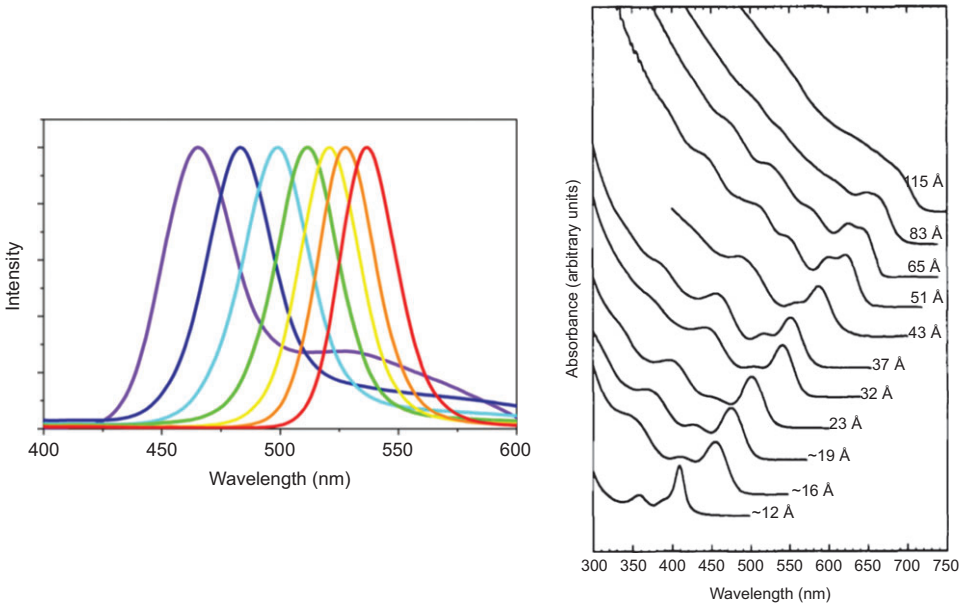

Figure 9 Emission spectra of CdSe QDs [49] (left) and the absorption spectra of CdSe QDs [50], both showing size-dependent features (right). Reprinted with permission from Ref. [50]. Copyright 2010 Wiley-VCH Verlag GmbH & Co. KgaA, Weinham.

4 The spectral design of light sources using semiconductor nanocrystal quantum dots

As mentioned in the previous section devoted to the color science and photometry, optimization of the white light spectrum is a complicated task that needs to be carried out in a manner specific to the application. For example, the design of an indoor light source requires successful color rendering, good spectral overlap with the human eye sensitivity function, and a warm white shade. On the other hand, a spectral design for outdoor lighting has different performance criteria. In this case, for example, the luminance has to be increased considering the changes in the eye sensitivity in the mesopic lighting levels. In addition, road lighting with a high CRI is thought to increase visual perception while driving. On the other hand, a light source affecting the human circadian cycle – more or less – requires a completely different spectral design. Since each application has different figure-of-merits and some applications have complicated trade-offs between the performance criteria, the emitters should be selected carefully for each specific application. For this purpose, narrow emitters such as QDs offer great potential, as they enable high flexibility in the spectral design, leading to high-quality light sources.

In this part of the review, we bring together the studies regarding the spectral design for indoor and outdoor applications using nanocrystal QDs as color-converter materials. For indoor lighting applications, the required spectral parameters and the trade-offs between relavent figure-of-merits are discussed. Moreover, a discussion of the power conversion efficiency potentials of the QD-integrated white LEDs follows. Under the heading of lighting design for outdoor applications, our recent studies on obtaining high mesopic luminance are summarized. Finally, we briefly touch on the QD-integrated white LED spectra with increased S/P ratios.

4.1 Spectral design for indoor lighting using nanocrystal QDs

In order to obtain warm white light sources exhibiting high CRI and high LER, the selected color components must be strategically selected. Knowing the trade-offs between these figure-of-merits is also helpful during the design of the light source. For this purpose, computational simulations were previously carried out by modeling the emission of nanocrystal QDs as a Gaussian spectrum [7]. The white light spectrum was generated using four color components, i.e., blue, green, yellow, and red. By changing the peak emission wavelength (WL), the full-width-at-half-maximum (FWHM), and the relative amplitude of each QD color component, in total 237,109,375 QD-integrated white LED (QD-WLED) spectra were tested in terms of photometric performance. Before investigating the results, a two-step threshold

was applied. First, the spectra possessing a CRI >80, an LER >350 lm/W_{opt}, and a CCT <4000 K were selected. These results were used for understanding the trade-offs between the performance metrics of the CRI, CCT, and LER. The second threshold was applied by increasing the CRI limit to 90 and the LER limit to 380 lm/W_{opt}.

The trade-offs between the CRI, LER, and CCT can be summarized in Figure 10, where the maximum obtainable CRI decreases as the LER increases. This trade-off is steeper when operating at a lower CCT for a warmer white shade. Moreover, the maximum obtainable CRI at a given LER requires warmer white shades up to LERs of ~370 lm/W_{opt}. After this LER value, the trade-off starts to change, and at even higher LERs, maximum obtainable CRIs are attained at cooler white shades.

In addition to the trade-offs, Ref. [7] summarizes the spectral requirements for obtaining high CRI and LER values by preserving the warm white emission using QDs. It has been found that the full-width-at-half-maximum of the red color component must be very narrow (~30 nm), in order to obtain high photometric performance. In addition, the relative amplitude of the red component should be strongly dominant in the spectrum (~430/1000), while the blue component must remain weak (~90/1000). Moreover, another critical parameter is found to be the peak emission wavelength of the red color component, which needs to be located in the proximity of 620 nm. This indicated value turns out to be very critical for achieving high performance. On the other hand, the average values found in the simulations indicate that blue, green, and yellow peak emission wavelengths have to be around 465, 528, and 569 nm, respectively. However, larger standard deviations obtained offer a flexibility in the choice of these peak emission wavelengths without having any significant loss in photometric performance. Similarly, the FWHM values of these color components reveal an average of ~44 nm with a standard deviation of ~8 nm, which again gives the designer flexibility in choosing these parameters. Finally, the averages of the relative amplitudes of the green and yellow components turn out to be 229/1000 and 241/1000, respectively, with standard deviations >70/1000. Compared to the standard deviations of blue and red (20/1000 and 49/1000, respectively), it is clear that selection of the green and yellow relative amplitudes is less critical for preserving the photometric performance of the QD-WLEDs. The spectrum, which is generated using the average values indicated above for the simulation thresholds of CRI >90, LER >380 lm/W_{opt}, and CCT <4000 K, has a CRI of 91.3, an LER of 386 lm/W_{opt}, and a CCT of 3041 K (Figure 11). The results of this study show that QD-WLEDs can possess very high CRI and LER values while maintaining a warm white shade.

Although the study in Ref. [7] stated that obtaining a photometrically efficient QD-WLED with good color rendition was possible, it did not consider the compatibility of the simulations to the ANSI standards [56] and did not investigate the rendering of test color sample 9 (R9), called the special CRI number 9, which may take very low values for LED lighting applications. These problems were addressed using a multi-objective evolutionary algorithm in the work of Zhong et al. [8] where R9≥90 and applicability to the ANSI and Energy Star standards were used as additional thresholds in addition to the performance limitations of CRI ≥80, LER ≥300 lm/W_{opt}, and 1500 K≤CCT≤6500 K. The optimal spectral parameters, which are in agreement with the ones stated in Ref. [7], for assessing whether CRI=95 and R9=95, leading to the highest LER, were given in Table 2, and corresponding spectra were given in Figure 12.

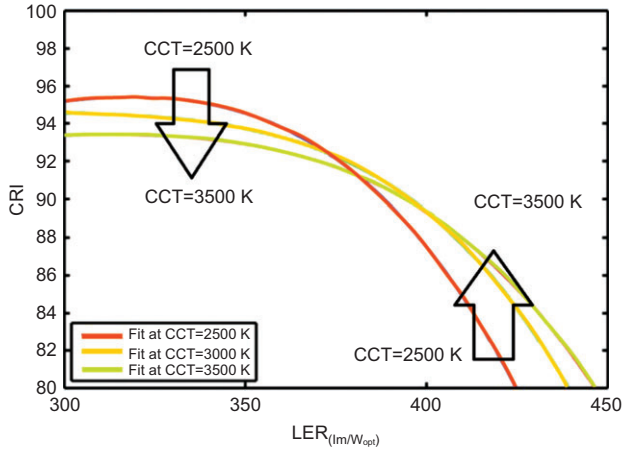

Figure 10 CRI vs. LER relationship at CCTs of 2500, 3000, and 4000 K [7, 55]. Reprinted with permission from Ref. [55]. Copyright 2011 Elsevier Ltd.

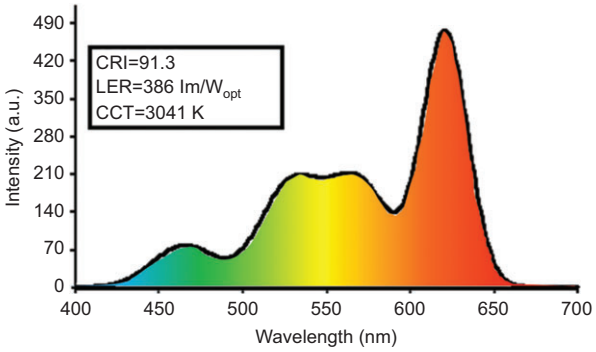

Figure 11 QD-WLED spectrum generated using the average values obtained by applying thresholds of CRI >90, LER >380 lm/W_{opt}, and CCT <4000 K along with its photometric performance [7].

Obtaining a QD-WLED spectrum possessing high photometric efficiency and high color quality does not mean that the light source is energy efficient. Therefore, the potential of these devices for energy efficiency has to be investigated separately by considering different architectures of QD films and their quantum efficiencies. This problem was addressed in Ref. [10] where QD-WLEDs were modeled as blue LEDs exciting green, yellow, and red QD films. Two basic architectures were studied in which green, yellow, and red QDs were (i) used to form a sequence of three separate coating layers on a blue LED (with green first, followed by yellow, and then red) and (ii) blended together to form a single coating layer on a blue LED. The power conversion efficiencies (PCEs) of the QD-WLEDs were calculated by assuming a blue LED chip having a PCE of 81.3% and using a color conversion scheme modeled with feedback loops. The calculations predicted that, when a layered architecture is used, quantum efficiencies of 43%, 61%, and 80% for the QDs are required to achieve luminous efficiencies (LEs) of 100, 150, and 200 lm/W_{elect}, respectively, for the spectra possessing an LER $\geq$380 lm/W_{opt}, a CRI $\geq$90, and a CCT $\leq$4000 K as in Ref. [7]. Moreover, the suitability of the spectra for the Energy Star and ANSI standards were satisfied, and spectra having an R9$\geq$70 have been included in the study. When the blended QD-WLED architecture is preferred, the required quantum efficiencies of the QDs need to increase to 47%, 65%, and 82%, respectively. Another important result revealed by this study was the effect of the energy down-conversion on the energy efficiency. It has been found that even if the quantum efficiency of the QDs are 100%, at least 17% of the optical energy is lost due to the Stokes shift as far as the photometrically efficient spectra exhibiting high color quality are considered. This corresponds to an LE of 315 lm/W_{elect} in the case of a perfect blue LED chip with a PCE of 100%.

4.2 Spectral design for outdoor lighting using nanocrystal QDs

The design of the light sources has to be undertaken with consideration of the specific application that it is intended for. For outdoor lighting conditions, the shade of the white light is not as significant as in the case of indoor lighting. More importantly, the sensitivity of the eye changes since the vision regime becomes mesopic under the luminance levels of road lighting. Therefore, a luminance calculation, which can be considered as an indicator of the perceived brightness, cannot reveal correct perception information if it is based on the photopic eye sensitivity function. Instead, the mesopic luminance should be considered by taking the changes in the eye sensitivity function into account.

A spectral recommendation study has been carried out considering these changes to enhance the mesopic luminance employing QD-WLEDs [57]. The first step of the study is the choice of the appropriate luminance levels which satisfy the conditions indicated in the road lighting standards of the UK [58] and the US [59]. For this purpose, four road lighting standards were chosen: Mesopic 1, which corresponds to a photopic luminance (L_p) of 0.50 cd/m^2, satisfies the freeway collector and local road

Table 2 Optimal spectral parameters of QD-WLEDs leading to the highest LERs satisfying CRI=95 and R9=95 at 1500 K$\leq$CCT$\leq$6500 K [8].

CCT (K)	2700	3000	3500	4000	4500	5000	5700	6500
Blue WL	462.5	462.3	461.6	460.9	460.2	461.1	460.4	459.7
Green WL	520.9	521.6	522.4	522.9	523.3	523.7	523.9	523.9
Yellow WL	566.0	566.0	566.2	566.6	567.0	566.7	567.4	568.2
Red WL	623.7	623.0	622.1	621.5	621.0	620.7	620.4	620.1
Blue FWHM	30	30	30	30	30	30	30	30
Green FWHM	30	30	30	30	30	30	30	30
Yellow FWHM	30	30	30	30	30	30	30	30
Red FWHM	30	30	30	30	30	30	30	30
Blue amplitude (%)	7.82	10.67	15.13	19.00	22.37	24.77	28.22	31.31
Green amplitude (%)	15.72	17.65	20.24	22.20	23.63	25.00	25.99	26.67
Yellow amplitude (%)	27.10	26.57	25.18	23.64	22.17	20.82	19.40	18.12
Red amplitude (%)	49.36	45.11	39.46	35.16	31.83	29.42	26.40	23.90
CRI	95	95	95	95	95	95	95	95
R9	95	95	95	95	95	95	95	95
CQS	93	94	94	93	93	93	93	93
LER (lm/W_{opt})	370	371	367	360	352	347	338	327

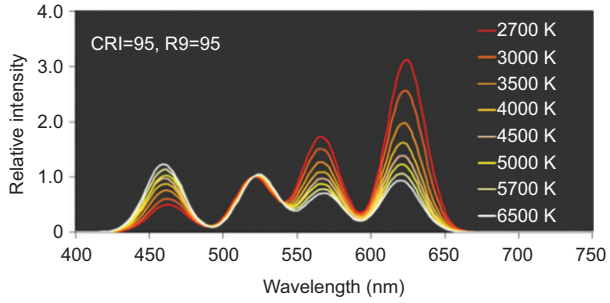

Figure 12 Optimal spectra of QD-WLEDs leading to the highest LERs satisfying CRI=95 and R9=95 at 1500 K≤CCT≤6500 K [8].

conditions of the US and the link road standard of the UK. The second luminance level (Mesopic 2) was chosen to be 0.80 cd/m^2, which fulfills the requirements of the expressway and major road standards of the US, and the secondary distributor standard of the UK. The third mesopic luminance level (Mesopic 3) was selected to be 1.25 cd/m^2 to satisfy the conditions of strategic route, major, and secondary distributors in the UK. Finally, Mesopic 4 corresponds to a luminance level of 1.75 cd/m^2, which is the appropriate level for satisfying motorway lighting standards of the UK.

The second step of the study is the investigation of the commercial light sources. For this purpose, the spectra of a cool white fluorescent lamp (CWFL), an incandescent lamp with a CCT of 3000 K, a metal-halide lamp (MH), a high-pressure sodium lamp (HPS), and a mercury vapor lamp (MV) were investigated along with the standard daylight source D65, which is included just for the purpose of comparison with daylight (Figure 13). The results showed that at lower radiances the CWFL achieves the highest mesopic luminance, whereas the HPS takes the lead at higher radiances. In accordance with this information, it has been found that the CWFL is the most efficient commercial light source for Mesopic 1 and 2 standards, whereas the HPS becomes the most efficient source for the remaining standards chosen in the study.

To investigate the performance of QD-WLEDs, a similar computation approach to Ref. [7] was followed. The QD-WLED spectra were generated such that they have the same radiances as the CWFL has for Mesopic 1 and Mesopic 2 conditions. For Mesopic 3 and 4, the QD-WLEDs having the same radiance as the HPS were generated. In order to reveal the spectral parameters necessary for achieving high mesopic luminance, new thresholds were determined in light of the requirements for mesopic lighting. The spectra, which can possess CRI and CQS values at or above 85 and satisfy the chromaticity difference requirements of ANSI [56], were selected. Additionally, all the spectra having mesopic luminance values less than the CWFL (for Mesopic 1 and 2) and the HPS (for Mesopic 3

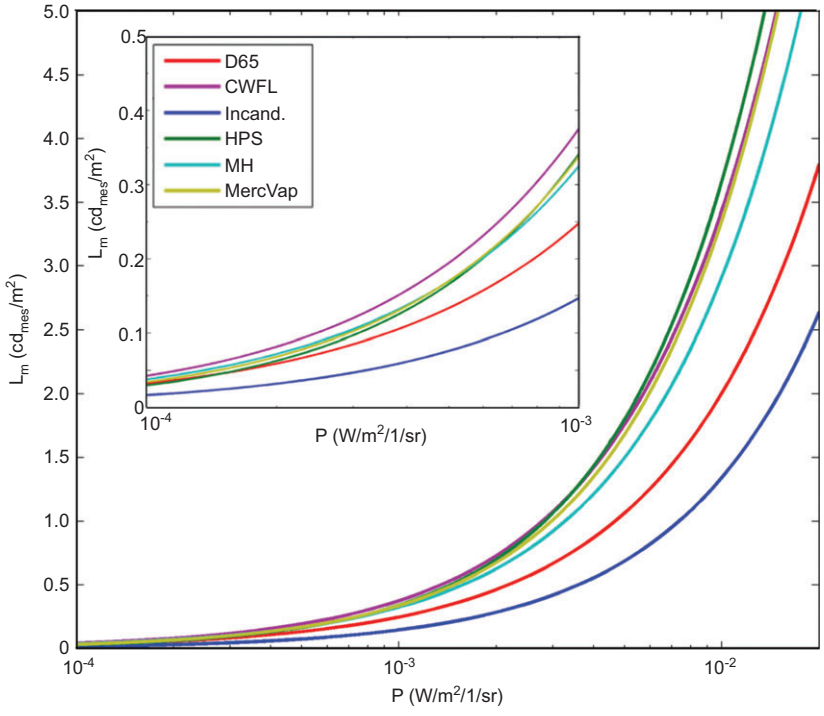

Figure 13 Mesopic luminance (L_{mes}) vs. radiance (P) for several conventional light sources: standard daylight source (D65), cool white fluorescent lamp (CWFL), incandescent lamp with a correlated color temperature of 3000 K (Incand.), metal-halide lamp (MH), high-pressure sodium lamp (HPS), and mercury vapor lamp (MercVap) [57].

and 4) were eliminated, and the best 100 spectra in terms of mesopic luminance were analyzed.

The maximum mesopic luminances achieved for the corresponding road lighting standards were given in Table 3 together with the CRI, CQS, and CCT values. The reported data indicates that achieving high mesopic luminance with good color rendition is still possible while remaining in the warm white region. Furthermore, it has been found that the mesopic luminance is maximized when the relative amplitudes of the blue, green, and yellow components are the same for the Mesopic 1 condition with the red component being three times stronger. However, under the conditions requiring higher photopic luminance, the blue component weakens, and the red component becomes more intense for achieving the highest luminance. Moreover, the peak emission wavelength of the blue component was found to be located at 460 nm, while this value is ca. 610 nm for the red component for the luminance values. Another interesting feature of this study is the fact that the red color component must be a very narrow-band emitter as in the case of indoor lighting.

To reveal the spectral conditions necessary for achieving high mesopic luminance, the average and standard deviations of the parameters, which belong to the QD-WLED spectra passing the threshold indicated above, were calculated. These results suggest that choosing the blue component close to 460 nm and the red component close to 610 nm is crucial for the increased mesopic luminance with good color rendition. In addition, the weight of the blue component should be around 150/1000, whereas the relative intensity of the red component should be chosen around 450/1000. Furthermore, it is not possible to use broad red emitters without falling below the performance limitations. Therefore, the red component should be designed using narrow-band emitters with bandwidths of ca. 30 nm. The green and yellow color components may have intermediate amplitudes; however, the designer has more flexibility in choosing the parameters of these color components in contrast with the case for blue and red.

5 Semiconductor nanocrystal quantum-dot-integrated white-light-emitting diodes (QD-WLEDs)

Until this section of this review, we have been surveying studies on the design of QD-WLEDs and their potential in terms of photometry and color quality. At this point in the review, we now begin summarizing the studies involving experimental demonstrations of QD-WLEDs. We first start by reviewing the QD-WLEDs based on the core-shell QDs. Under this heading, Cd-free QD-based white LEDs as well as white LEDs using phosphors and QDs together are included in addition to the LEDs based on Cd-containing QDs. Subsequently, we continue with a white-light-emitting diode using transition-metal-doped QDs, which are a relatively new class of QD-WLEDs. Finally, we will discuss the white LEDs based on only core QDs.

Following the first demonstrations of the use of color-converting QDs on LEDs [60–63], QD-WLEDs have been studied extensively for better color quality and photometric efficiency and the overall performance has been improved over the past years. One of the first studies employed CdSe/ZnS QDs on an InGaN/GaN quantum-well blue LED [63]. In this study, Demir and his group demonstrated the tunability of the CCT between 2692 K and 11,171 K along with that of the CRI between 14.6 and 71.0 using combinations of cyan, green, orange, and red QDs on the blue LED chip. One year later, the researchers enhanced the performance of the device using the same material system [64]. It was reported that the QD-WLEDs reach a CRI of 81 while having an LER of 323 lm/W_{opt} and a CCT of 3190 K. The spectrum of the white LED achieving this performance is given in Figure 14.

This performance of the QD-WLEDs was improved by using green, yellow, and red CdSe/ZnS QDs, having in toluene respective peak emission wavelengths of 528, 560, and 609 nm, on a blue InGaN/GaN LED chip [65]. This particular device achieved an LER of 357 lm/W_{opt} together

Table 3 Radiance (P), photopic luminance (L_p), mesopic luminance (L_{mes}), CRI, CQS, and CCT of the QD-WLED spectra exhibiting the highest mesopic luminance for the simulated four mesopic road lighting standards, together with scotopic and photopic vision regimes [54].

	P [mW/(m²sr)]	L_p (cd/m²)	L_{mes} (cd_{mes}/m²)	CRI	CQS	CCT (K)
Scotopic	1.50×10^{-2}	0.005	0.010	85.0	88.4	4969
Mesopic 1	1.47	0.577	0.625	85.8	85.1	3417
Mesopic 2	2.36	0.932	0.980	85.9	85.1	3243
Mesopic 3	3.39	1.340	1.393	85.9	85.1	3243
Mesopic 4	4.74	1.886	1.930	86.1	85.2	3164
Photopic	13.6	5.386	5.386	87.1	85.3	3033

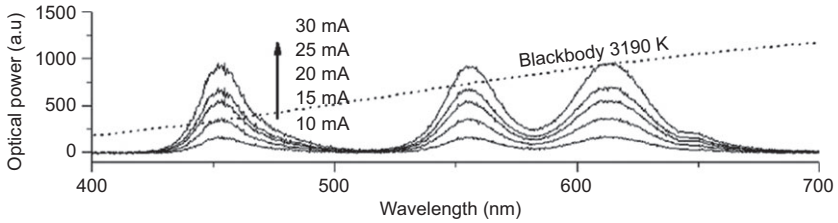

Figure 14 Measured spectra of the white LED fabricated by hybridizing CdSe/ZnS QDs on blue InGaN/GaN LED. This QD-WLED exhibits the following performance: CRI=81, LER=323 lm/W_{opt}, and CCT=3190 K [64]. Reprinted with permission from Ref. [64]. Copyright 2008 American Institute of Physics.

with a CRI of 89.2 and a CCT of 2982 K. The spectrum, color coordinates, and the photograph of this QD-WLED are presented in Figure 15. In another study of Nizamoglu et al. CdSe/ZnS QDs were used in white LEDs to achieve a high S/P ratio together with a high CRI [66]. In that particular study, the designed QD-WLED exhibited an S/P ratio of 3.04 with a CRI of 71 at CCT=45,000 K.

In addition to the CdSe/ZnS core/shell structures, QDs with other architectures were also investigated for QD-WLED fabrication. Among them, an interesting one is the QD-WLED integrated with (CdSe)ZnS/CdSe (core)/shell/shell QDs, which has a dual-color emission [67]. While the red emission comes from the core of the QD, the second shell was expected to emit in the green. Finally, white light emission was realized by integrating these QDs with an InGaN/GaN blue LED (Figure 16). This device exhibited values of CRI=75.1, LER=278 lm/W_{opt}, and CCT=3929 K.

While the studies on increasing the performance of the QD-WLEDs continue, research efforts began to focus on synthesizing QDs in environmentally friendly and cost-effective ways. One of the most important problems of the QDs is the use of phosphines in the synthesis, which in turn increases the cost of the QDs and makes them harmful to the environment. To address this problem, Wang et al. developed a phosphine-free synthesis route for CdSe/CdS/ZnS core/shell/shell QDs in paraffin liquid and used these materials in white LEDs [68]. They synthesized green QDs emitted at 512 nm with a quantum efficiency (QE) of 55%, whereas the yellow- and red-emitting QDs had peak emission wavelengths of 563 nm and 615 nm, respectively, and QEs of 65% and 40%, respectively. The fabricated device exhibited a high CRI of 88 and warm white emission with a CCT of 3865 K while achieving a luminous efficiency (LE) of 32 lm/W_{elect}.

Another significant problem of the common QD materials is their Cd content. To obtain environmentally friendly QDs, new techniques are under development for the synthesis of Cd-free QDs. One of these QDs is the CuInS/ZnS core shell QD [69], the emission peaks of which can be adjusted by controlling its indium content. In Ref. [69], CuInS/ZnS QDs with a Cu/In ratio of 1/4 were used and white light emission was obtained having a CRI of 72 and an LE of 79.3 lm/W_{elect}. The spectrum of the resulting LED is depicted in Figure 17. In another work of Song

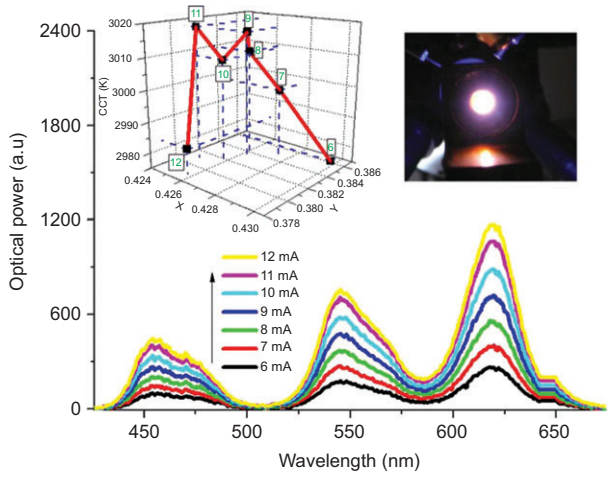

Figure 15 Measured spectra, chromaticity coordinates, and photograph of the CdSe/ZnS QD-integrated white LED exhibiting figure-of-merits of CRI=89.2, LER=357 lm/W_{opt}, and CCT=2982 K [65].

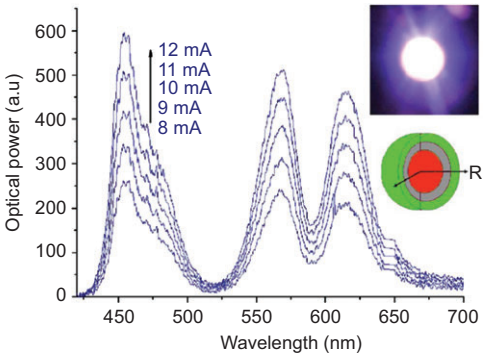

Figure 16 Spectra and photograph of the (CdSe)ZnS/CdSe (core) shell/shell QD-integrated white LED [67]. Reprinted with permission from Ref. [67]. Copyright 2008 American Institute of Physics.

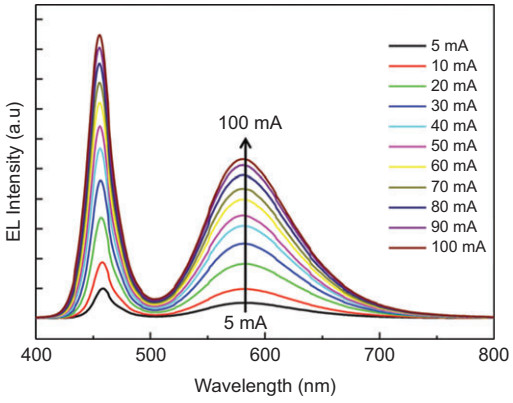

Figure 17 Spectra of the QD-WLED based on CuInS/ZnS core/shell QDs exhibiting a CRI of 72 and an LE of 79.3 lm/W_{elect} [69]. Reprinted with permission from Ref. [69]. Copyright 2012 Wiley-VCH Verlag GmbH & Co. KgaA, Weinham.

et al. yellow- and orange-emitting CuInS/ZnS QDs were employed for the generation of white light [70]. Compared to Ref. [69], the CRI was enhanced to a value of 80–82 while achieving an LE of 52 lm/W_{elect}.

Another important Cd-free QD, which has been extensively studied by researchers, is the InP/ZnS core/shell QDs. Recently, significant developments were achieved in the synthesis and device applications of these materials. In the work of Mutlugun et al. a white LED was demonstrated, which possesses a CRI of 89.3 at a CCT of 2982 K with an LER of 254 lm/W_{opt} [71]. The spectrum and a photograph of this particular QD-WLED are given in Figure 18.

An important problem associated with InP/ZnS, InP/ZnSe, and InP/ZnSSe QDs is the lattice mismatch between the core and shell materials, which limits the improvement of quantum efficiency. As a solution, Kim et al. proposed the InP/GaP/ZnS core/shell/shell QDs [72]. These QDs achieved a quantum efficiency of 85%, and the white LEDs made from them were demonstrated by blending the QDs with yttrium aluminum garnet (YAG) phosphor. This QD-WLED exhibited a CRI of 80.56 at a CCT of 7864 K with an LE of 54.71 lm/W_{elect}. It is worth mentioning here that the incorporation of QDs in phosphors is not peculiar to Ref. [72]. For example, Woo et al. used Sr_2SiO_4:Eu green phosphor together with red QDs of CdSe/CdS/CdZnS/ZnS on an InGaN/GaN blue LED [73]. The QDs had an emission peak at 617 nm with a full-width at half-maximum of 32 nm, and a quantum efficiency above 55%. This device exhibited a CRI of 88.4 with a 71.2 lm/W_{elect} luminous efficiency at a CCT of 8684 K. The spectrum and the photograph of this particular device are shown in Figure 19.

In addition to the simultaneous use of QDs and phosphors as color converters on an epitaxially grown blue LED, the QDs were also employed as down-converters on electroluminescent phosphors. In the work of Kundu et al. the so-called giant CdSe/CdS QDs with 16 monolayers of shells were used as the red emissive nanophosphor at 625 nm, while the green emission at 570 nm originated from InP/ZnSe QDs on an electroluminescent blue phosphor powder of Cu/Cl-doped ZnS [74]. By utilizing these materials, CCTs of the white LED were tuned between 3200 and 5800 K. The schematic of the device and the electroluminescence spectra are presented in Figure 20.

The incorporation of phosphors together with QDs was also investigated in white LEDs using doped QDs [54]. Since these special QDs exhibit a large Stokes shift; that is, since the emission and absorption spectra of these nanoparticles are well-separated from each other, they do not suffer from the reabsorption problem. Therefore, they are promising materials for use in color-conversion LEDs. To this end, Wang et al. integrated Cu-doped CdS/ZnS

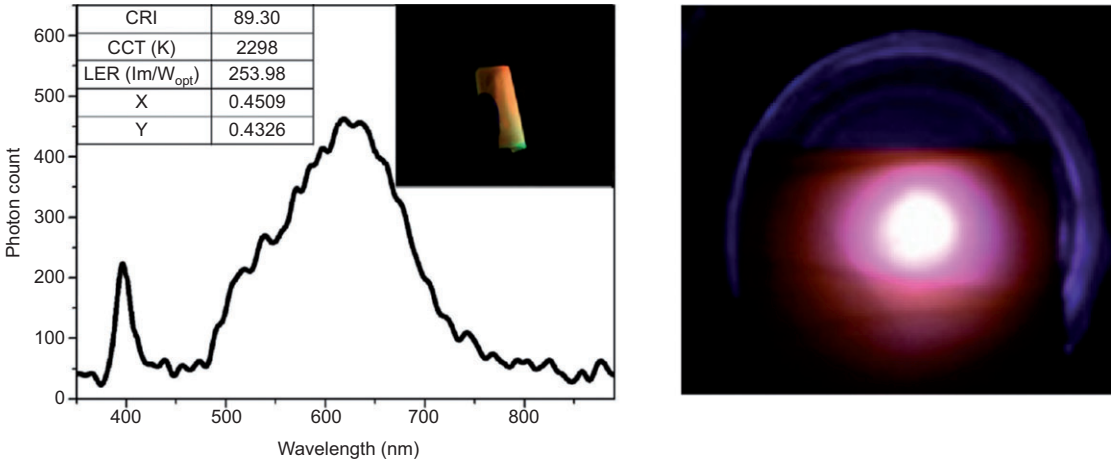

Figure 18 Spectra of the QD-WLED based on InP/ZnS QDs, its colorimetric and photometric performance (left), and a photograph of the QD-WLED (right) [71]. Reprinted with permission from Ref. [71]. Copyright 2012 American Chemical Society.

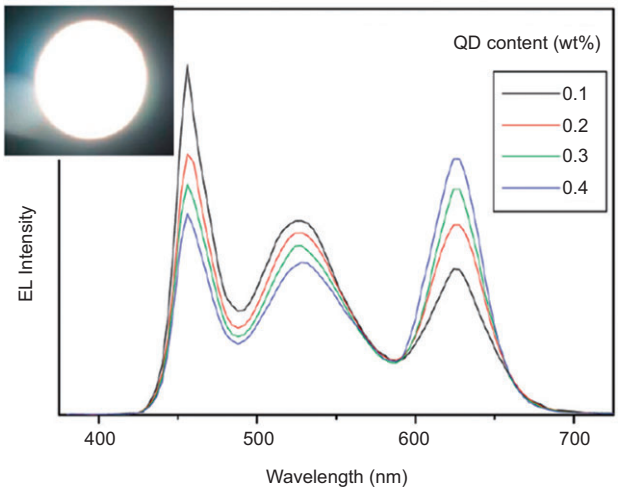

Figure 19 Spectra of a QD-WLED, which is designed using Sr_2SiO_4:Eu green phosphor and red QDs of CdSe/CdS/CdZnS/ZnS, at 30 mA with varying QD concentrations [73]. The inset shows a photograph of the device. Reprinted with permission from Ref. [73]. Copyright 2011 American Chemical Society.

QDs and YAG:Ce phosphors on a blue-emitting LED chip to generate white light. Without any doping, CdS/ZnS QDs normally emit in the blue regime and their absorption starts close to this emission peak and increases toward the UV. When these QDs are doped with a transition metal like Cu, the emission mechanism is dominated by the states introduced by Cu, and therefore, a red-emitting QD is obtained while the absorption spectrum before the doping is still preserved. Therefore, a large Stokes shift is introduced. In the study of Wang et al. these QDs emitting around 650 nm were used together with the green-emitting YAG:Ce phosphor on an InGaN/GaN blue LED.

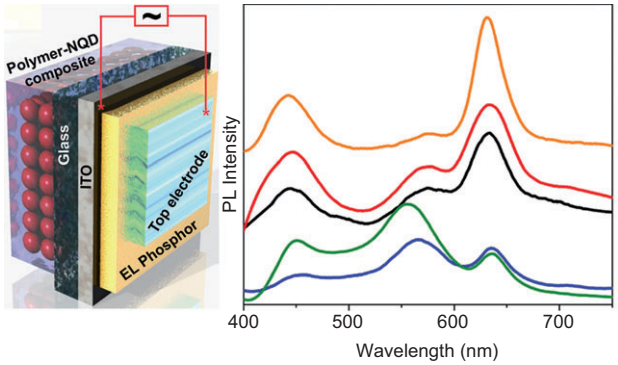

Figure 20 Device architecture of AC driven electroluminescent phosphor integrated color converting QDs (left) and its electroluminescence spectra (right) of white LEDs having different concentrations of green and red QDs [74]. The blue, green, black, red, and orange spectra exhibit CCTs of 4200, 5800, 4403, 4686, and 3200 K, respectively. Reprinted with permission from Ref. [74]. Copyright 2012 American Chemical Society.

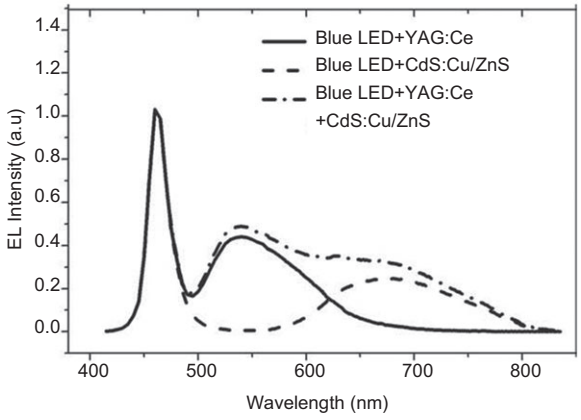

Figure 21 Spectra of the LED integrated with YAG:Ce phosphor and Cu:CdS/ZnS QDs, the version integrated with only the YAG:Ce phosphor, and the phosphor-free Cu:CdS/ZnS QD-integrated LEDs [69]. Reprinted with permission from Ref. [69]. Copyright 2012 Wiley-VCH Verlag GmbH & Co. KgaA, Weinham.

The resulting white LED spectrum exhibited a CRI of 86 with an R9 value of 90 and an LE of 37.4 lm/W_{elect}. The electroluminescence spectrum of this device, a version integrated with only the YAG:Ce phosphor, and a version integrated only with the QDs are given in Figure 21.

Although the QDs in general possess a very narrow emission band, obtaining a broader emission is also possible by the introduction of trap states or surface states, especially when small-sized QDs are used. Therefore, this emission mechanism can be used for obtaining white light emission in QD-WLEDs. Nizamoglu et al. applied this idea to the CdS QDs having a sharp blue emission accompanied with a broad yellow emission [75]. By integrating these QDs on a near-UV-emitting InGaN/GaN LED, spectral tunability of the QD-WLEDs

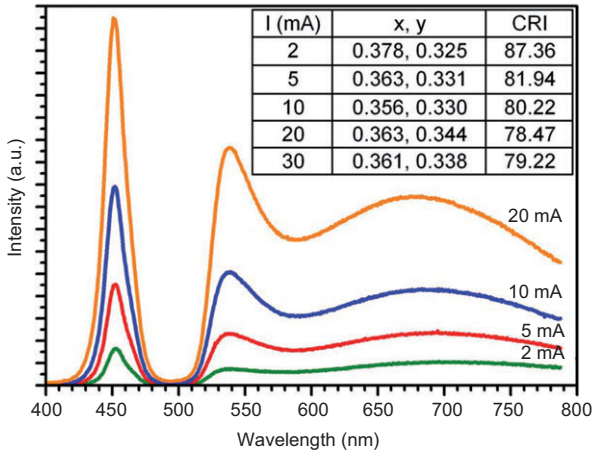

Figure 22 Spectra of CdSe QDs integrated on a blue LED and the resulting CRIs of the QD-WLED for injection currents from 2 to 30 mA [76].

was achieved with CRIs ranging from 57.3 to 74.9 and CCTs ranging from 34,463 K to 4718 K. A similar study was carried out by Chandramohan et al. using CdSe-core QDs having a diameter of 2.5 nm integrated on a blue LED emitting at 460 nm [76]. The resulting device exhibited a CRI of 87.36 at 2 mA and a CRI of 79.22 at 30 mA.

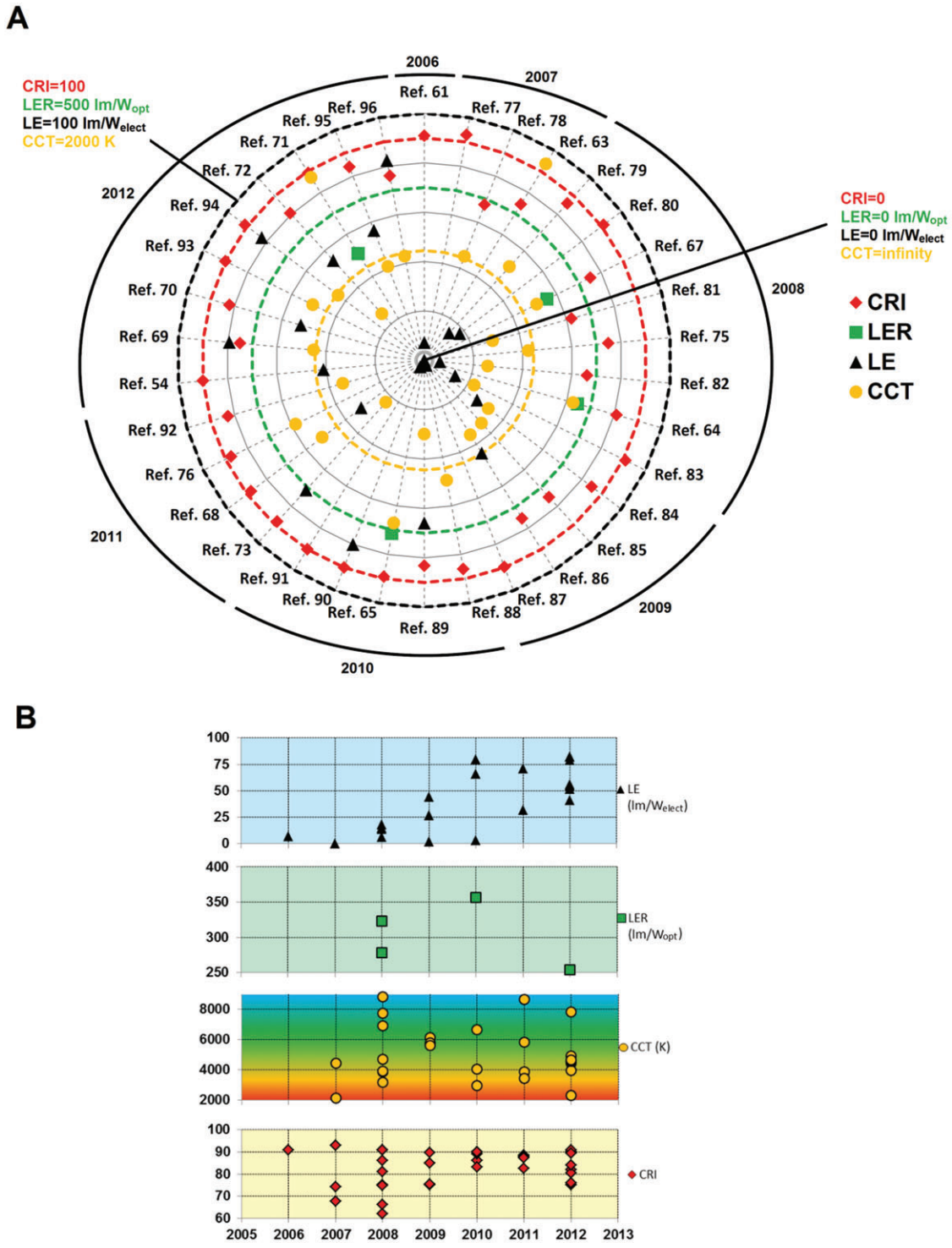

Figure 23 (A) Performance landscape of the QD integrated white LEDs categorized according to years. The center point corresponds to CRI=0, LE=0 lm/W_{opt}, LE=0 lm/W_{elect}, and CCT=infinity, while the outer rim indicates CRI=100, LER=500 lm/W_{opt}, LE=100 lm/W_{elect}, and CCT=2000 K. CCT points are presented on this graph by calculating 200,000/CCT. The red dashed circle shows the location of CR=90; the green dashed circle, LER=350 lm/W_{opt}; and the black dashed circle, LE=100 lm/W_{elect}; and the yellow dashed circle, CC=4500 K. (B) Evolution of CRI, LER, LE, and CCT in time.

The emission spectra belonging to these QD-WLEDs are given in Figure 22.

We close this section with an overview of the reported experimental studies on QD-WLEDs. In Figure 23(A), a collection of CRI, CCT, LER, and LE of the experimentally realized white LED prototypes is presented [54, 61, 63–65, 67–73, 75–96]. The important limits for these figure-of-merits are indicated using dashed circles. For obtaining warm white light, CCTs of the light sources should be located outside the yellow dashed circle. Similarly, CRIs of the sources should be on or outside the red dashed circle indicating CRI >90 for realizing successful color rendering whereas the green and black dashed circles indicate the LER=350 lm/W_{opt} and LE=100 lm/W_{elect} boundaries, respectively. Achieving performance beyond these dashed circles can be considered as the targeted performance for QD-WLEDs in the future. Here, the improvement on LE attracts special attention. While an LE below 1 lm/W_{elect} had been realized in the early devices, this value was increased above 80 lm/W_{elect} in more recent demonstrations. Moreover, significant improvements were observed in terms of photometric optimization by achieving CRI >90, LER >350 lm/W_{opt}, and CCT <4500 K, simultaneously. However, LE ≥100 lm/W_{elect} limit should be satisfied together with high color quality and photometric efficiency, which has been predicted to be feasible [10]. Additionally, for clarity, the evolution of these individual figure-of-merits in time is also depicted separately in Figure 23(B).

6 QD-integrated LEDs as display backlights

In addition to the general lighting applications, QDs offer great potential for display backlights as well. This is mainly because of the color control and narrow emission of QDs, which in turn allow for reproduction of a large number of colors in liquid crystal displays (LCDs). In Figure 24, the National Television System Committee (NTSC) standard color gamut, which indicates the subset of all colors that should be generated, is given along with the potential color gamut of displays using QD-integrated backlights. The black lines in the graph stand for the chromaticity coordinates of the QDs emitting between 460 and 700 nm with FWHM values ranging from 30 to 100 nm. Clearly, correct combinations of QDs can exhibit a much larger color gamut than the color gamut standardized by the NTSC. This means that, by using QD-integrated display backlights, more colors can be generated by LCD televisions and consequently, the quality of the images displayed can be enhanced significantly and richer viewing experience can be achieved.

Before moving to the display applications of QDs, it is worth commenting here on the required properties of the QDs in light of the NTSC color space in Figure 24. If a red-green-blue (RGB) light source is designed, the FWHM of the QDs should be at most 50 nm. Otherwise, the green end of the NTSC triangle cannot be included. Moreover, the blue emission should be generated with a source having a FWHM of <70 nm. Since the blue color component of QD-WLEDs mostly stems from the blue LED, this requirement is not a challenging restriction. In addition, the red QDs emitting around 610 nm can easily satisfy the NTSC color gamut requirements. A QD-WLED employing four or more color components can easily achieve color gamuts much larger than the NTSC standards indicate. However, narrow emissions from the green and blue components are still required.

QD-WLEDs were demonstrated as display backlights by Jang et al. [9] In this study, an InGaN/GaN blue LED was used as the blue color source, while CdSe/ZnS/CdSZnS and CdSe/CdS/ZnS/CdSZnS core/multi-shell

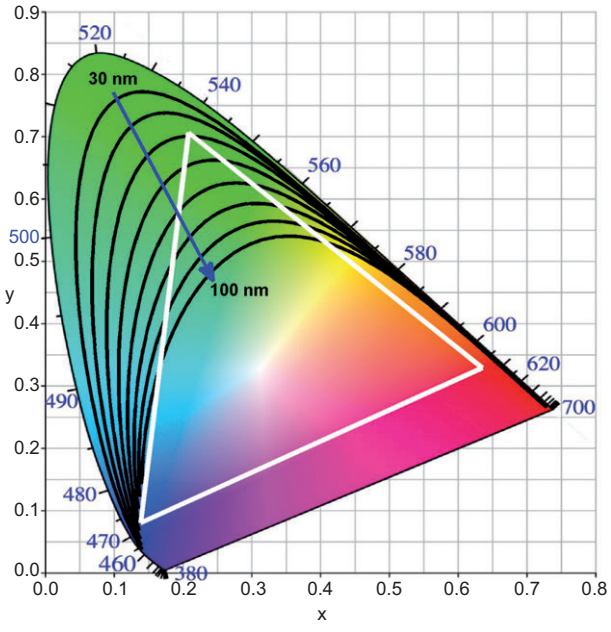

Figure 24 CIE 1931 chromaticity indicating the NTSC color gamut (white triangle), and color coordinates of QDs having full-width half-maximum values between 30 and 100 nm with peak emission wavelengths ranging from 460 to 700 nm (black lines). The blue numbers given around the perimeter of the chromaticity diagram are located at the color coordinates of the corresponding monochromatic light. The chromaticity diagram in the background was taken from Ref. [97] and the information regarding QD emission and the NTSC color space was added to this image.

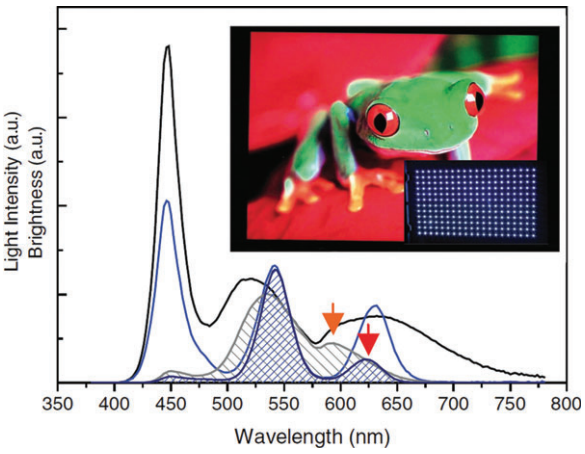

Figure 25 Emission spectra of the QD-integrated white LED (blue solid line) and a phosphor-based white LED used for comparison (black solid line). The inset shows an image on an LCD TV panel backlit with QD-WLEDs [9]. Reprinted with permission from Ref. [9]. Copyright 2010 Wiley-VCH Verlag GmbH & Co. KgaA, Weinham.

QDs were the sources of the green and red emission, respectively. The quantum efficiency of these QDs approached unity in solution, and in-film efficiencies of more than 70% were achieved. This device exhibited an LE of 41 lm/W_{elect} by maintaining the initial efficiency for more than 2200 h. This QD-WLED was used as the backlight of a 41-inch LCD TV, and 100% reproduction of the NTSC color gamut was realized. The spectrum of the QD-WLED and a display image of the LCD TV are given in Figure 25.

The QD-WLED presented in Ref. [9] was prepared by blending the QDs with silicone. Kim et al. applied a different methodology during the fabrication by using transfer printing [98]. In this study, microstrips of red, green, and blue QDs were generated. The electroluminescent LEDs are shown in Figure 26, together with a summary of the fabrication procedure. Although this device employs the electroluminescence of the QDs, which is not the focus of

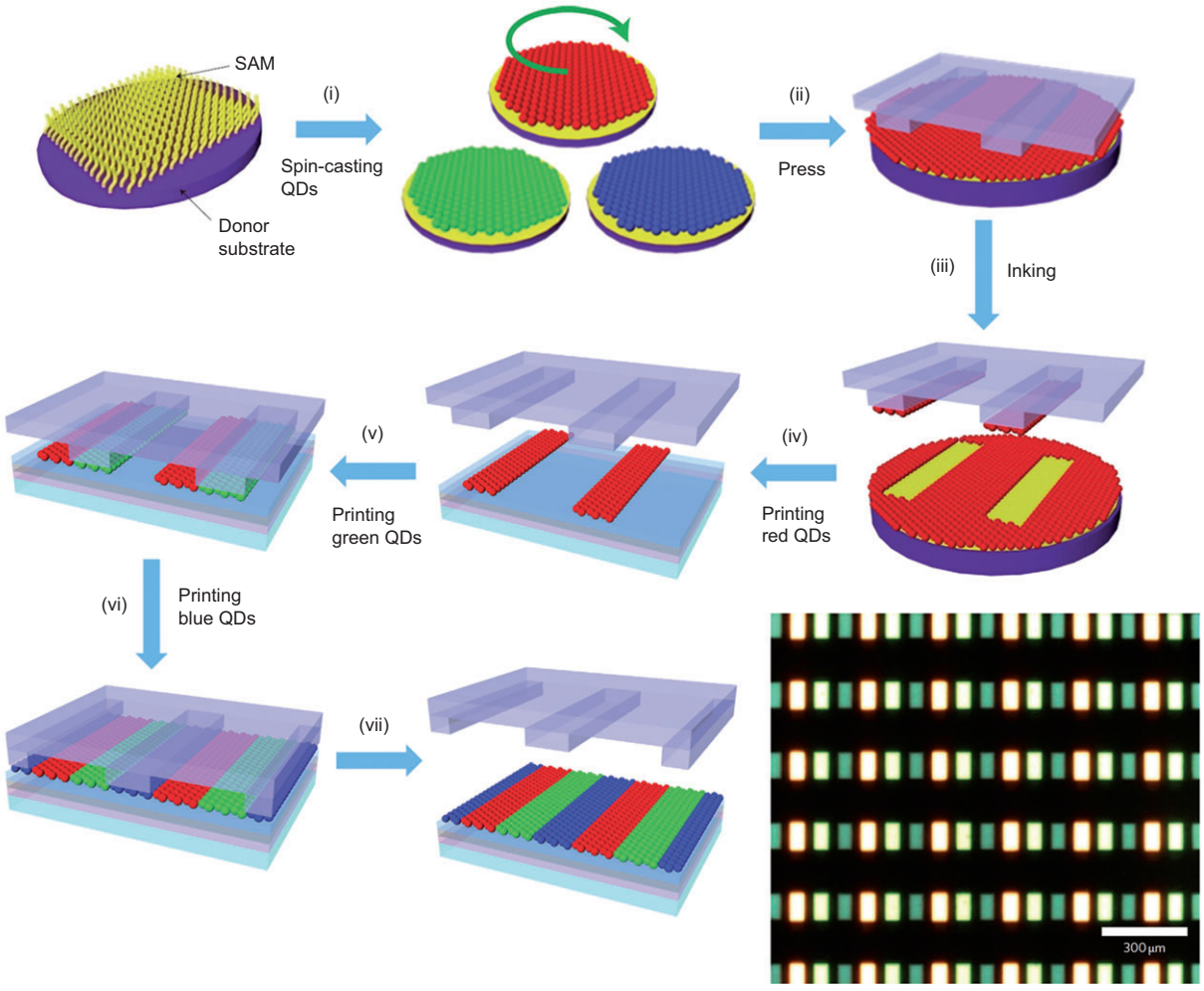

Figure 26 Illustration of transfer printing procedure to fabricate an electroluminescent display using QDs [98]. Reprinted with permission from Ref. [98]. Copyright 2011 Nature Publishing Group.

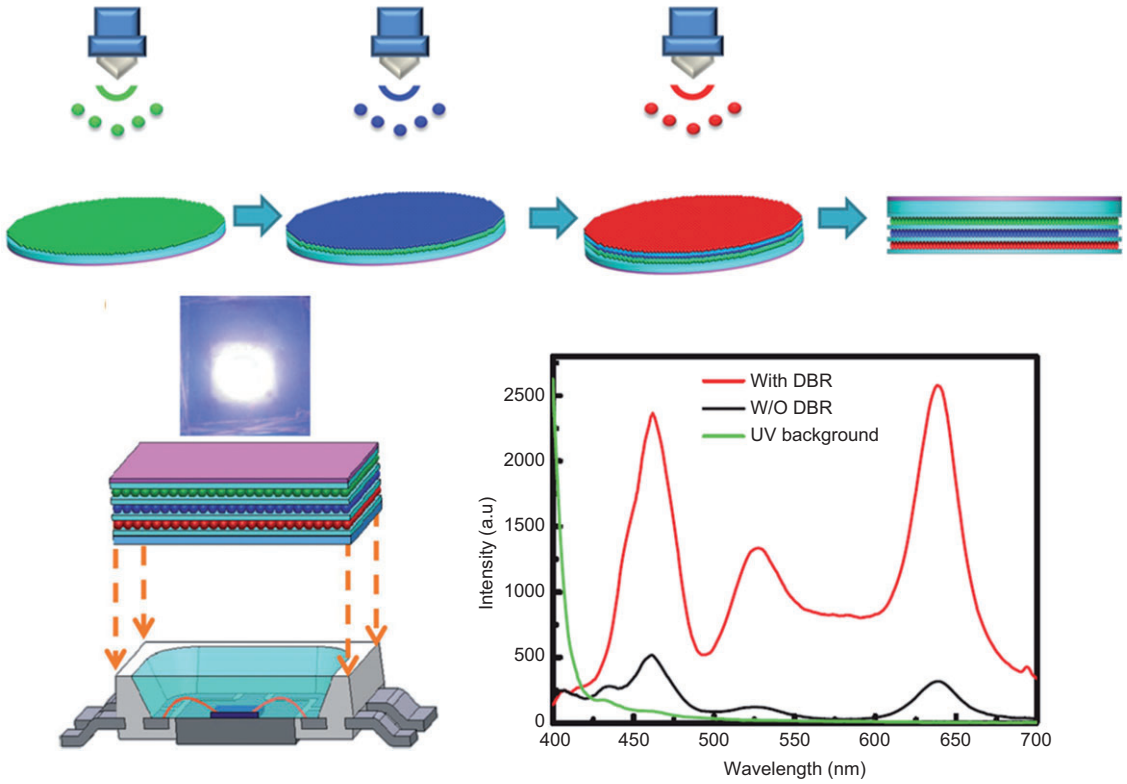

Figure 27 Illustration of fabrication procedure (top) and device schematics of the QD-WLED (left) and the emission spectra of the resulting LEDs with and without the DBR (right) [99]. Reprinted with permission from Ref. [99]. Copyright 2012 Wiley-VCH Verlag GmbH & Co. KgaA, Weinham.

this review, we included this study in this review because of the novelty in its fabrication method and its applicability to color-conversion LEDs.

Another method for fabricating QD-LEDs employed spray-coating of red, green, and blue QDs [99]. In this case, red CdSe QD emitting at 635 nm, green CdZnSeS QDs emitting at 546 nm, and CdS QDs emitting at 460 nm were spray-coated on PDMS and integrated on a UV LED. Moreover, a distributed Bragg reflector (DBR) made of HfO_2 and SiO_2 was added to recycle the UV radiation. The resulting QD-WLED achieved a color gamut 1.2 times larger than the NTSC standards. Schematic illustrations of the fabrication and the device structure are shown in Figure 27 together with the emission spectra of the QD-WLED with and without the DBR.

7 Conclusion and future outlook

In conclusion, we have covered the recent developments in quantum-dot-integrated white LEDs (QD-WLEDs) based on color conversion. First, we provided an introduction to the color science and photometry, which include the necessary information for evaluating the performance of white light sources. Subsequently, we discussed the spectral design of QD-WLEDs and the necessary conditions for high performance. The experimental demonstration of QD-WLEDs for general lighting applications and displays followed.

The studies summarized in this review indicate that QD-WLEDs offer great potential for indoor and outdoor lighting applications. In contrast to other conventional sources like phosphor-based white LEDs, fluorescent and incandescent lamps, these devices can exhibit successful color rendition with CRIs close to 90, good overlap with the human eye sensitivity curve with luminous efficacy of optical radiation higher than 350 lm/W_{opt} with a warm white shade indicated by correlated color temperatures <4500 K, simultaneously [7]. On top of this high photometric performance and high color quality, the synthesis of efficient QDs enabled the development of QD-WLEDs achieving luminous efficiencies close to 80 lm/W_{elect} [69], while there is still significant space for development up to 315 lm/W_{elect}, which was theoretically shown to be possible while maintaining the high color quality and photometric efficiency [10]. Moreover, their use in displays enables the reproduction of colors very successfully. Since QDs can have

very narrow emission bands, it was shown that a color gamut larger than what is required by the NTSC standards can be easily achieved by employing QD-WLEDs as display backlights.

While the QD-WLEDs offer such a high potential for widespread use in the future, their thermal stability and photostability must be further studied. As one of the important challenges, the thermal droop needs to be addressed, accompanied with aging and lifetime tests. Various strategies including using silica shells and silica matrix are possible for protecting QDs against heat. Also, the remote phosphor application is another approach to circumvent or reduce thermal issues. In addition, QDs are currently not sufficiently resistant to the conditions present during the encapsulation process. Either they need to be made stronger against the conditions occurring during the encapsulation of host polymers or new encapsulants must be developed so that the QDs are not affected adversely during this process. This will enable making more efficient QD films. Considering the significant improvements to obtaining efficient but also environment friendly Cd-free QDs, which was one of the biggest challenges a few years ago, the development of a proper encapsulant may be expected in the near future. With that advance, the QD-WLEDs will be ready for widespread use.

Acknowledgements: This work has been financially supported in part by National Research Foundation of Singapore under NRF-CRP6-2010-02 and NRF RF 2009-09, and in part by ESF EURYI, EU FP7 Nanophotonics4Energy NoE, and TUBITAK under Project Nos. EEEAG 110E217. H. V. D. acknowledges additional support from TUBA-GEBIP, and T. E. acknowledges TUBITAK-BIDEB.

Received October 3, 2012; accepted December 21, 2012; previously published online January 22, 2013

References

[1] Irvine-Halliday D, Peon R, Doluweera G, Platonova A, Irvine-Halliday G. Solid-state lighting: the only solution for the developing world. SPIE Newsroom 2006.
[2] US Environmental Protection Agency Energy Star. Saving energy by proxy. Off the Charts 2006:5–7.
[3] Peon R, Leon S, Irvine-Halliday D. Solid state lighting for the developing world: the only solution. Fifth International Conference on Solid State Lighting 2005;5941:59410N–15.
[4] U.S. Department of Energy, Office of Energy Efficiency and Renewable Energy, Building Technologies Program Energy Savings Estimates of Light Emitting Diodes in Niche Lighting Applications, 2011.
[5] Graydon O. The new oil? Nat Photonics 2011;5:1.
[6] Erdem T, Demir HV. Semiconductor nanocrystals as rare-earth alternatives. Nat Photonics 2011;5:126.
[7] Erdem T, Nizamoglu S, Sun XW, Demir HV. A photometric investigation of ultra-efficient LEDs with high color rendering index and high luminous efficacy employing nanocrystal quantum dot luminophores. Opt Express 2010;18:340–7.
[8] Zhong P, He G, Zhang M. Optimal spectra of white light-emitting diodes using quantum dot nanophosphors. Opt Express 2012;20:9122–34.
[9] Jang E, Jun S, Jang H, Lim J, Kim B, Kim Y. White-light-emitting diodes with quantum dot color converters for display backlights. Adv Mater 2010;22:3076–80.
[10] Erdem T, Nizamoglu S, Demir HV. Computational study of power conversion and luminous efficiency performance for semiconductor quantum dot nanophosphors on light-emitting diodes. Opt Express 2012;20:3275–95.
[11] Rogach AL, Gaponik N, Lupton JM, Bertoni C, Gallardo DE, Dunn S, Pira NL, Paderi M, Repetto P, Romanov SG, O'Dwyer C, Sotomayor Torres CM, Eychmüller A. Light-emitting diodes with semiconductor nanocrystals. Angew Chem Int Ed 2008;47:6538–49.
[12] Wood V, Bulović V. Colloidal quantum dot light-emitting devices. Nano Rev 2010;1:5202.
[13] Wyszecki G, Stiles WS. Color science: concepts and methods, quantitative data and formulae. NY: Wiley-Interscience; 2000.
[14] Webvision, The Organization of the Retina and Visual System, (Accessed Sep 5, 2012, at http://webvision.med.utah.edu/book/part-i-foundations/simple-anatomy-of-the-retina/)
[15] Stell WK. The morphological organization of the vertebrate retina. Physiology of photoreceptor organs (A 73-23301 09-04). Berlin: Springer-Verlag; 1972:111–213.
[16] Schubert EF. Light-emitting diodes. New York: Cambridge University Press; 2006.
[17] CIE Commission Internationale de l'Éclairage Proceedings, 1931. Cambridge: Cambridge University Press; 1932.
[18] Brown TG, Creath K, Kogelnik H, Kriss M, Schmitt J, Weber MJ. The optics encyclopedia: basic foundations and practical applications. Berlin: Wiley-VCH; 2004.
[19] CIE Commission Internationale de l'Éclairage Proceedings, Colorimetry. CIE 15.2;1986.
[20] Raynham P, Saksvrikrønning T. White light and facial recognition. The Lighting J 2003;68:29–33.
[21] Davis W, Ohno Y. Color quality scale. Opt Eng 2010;49:033602.
[22] Thornton WA. Color-discrimination index. J Opt Soc Am 1972;62:191–4.
[23] Fotios SA. The perception of light sources of different color properties. PhD Thesis, University of Manchester, Institute of Science and Technology, UK; 1997.
[24] Xu H. Color-rendering capacity of illumination. J Opt Soc Am 1983;73:1709–13.
[25] Hashimoto K, Nayatani Y. Visual clarity and feeling of contrast. Color Res Appl 1994;19:171–85.
[26] Judd DB. A flattery index for artificial illuminants. Illum Eng 1967;62:593–8.
[27] CIE Commission Internationale de l'Éclairage Proceedings, Colorimetry. CIE 15; 1971.

[28] CIE Commission Internationale de l'Éclairage Proceedings. Method of measuring and specifying color-rendering of light sources. CIE 13.3; 1995.
[29] Li C, Luo MR, Rigg B, Hunt RWG. CMC 2000 chromatic adaptation transform: CMCCAT2000. Color Res Appl 2002;27:49–58.
[30] Light Quality, Energy Star. (Accessed Sep 5, 2012 at http://www.energystar.gov/ia/products/lighting/fixtures/fixture_guide//person_colortemp.jpg).
[31] CIE Proceedings, 1951.
[32] OSRAM Sylvania Corporation Technical Report, Lumens and mesopic vision, 2000.
[33] Johnson LB. Upper limit of mesopic vision. Trans Illum Eng Soc 1937;32:646–50.
[34] LeGrand Y. Handbook of sensory physiology, Vol. VII/4: Visual psychophysics. In: Jameson D, Hurvich L, editors. Berlin: Springer Verlag, 1972.
[35] Kokoschka S. Das V(λ)-Dilemma in der Photometrie. Proceedings of 3. Internationales Forum für den lichttechnischen Nachwuchs, Technische Universität Illmenau, 1997.
[36] Illumination Engineering Society of America. IESNA lighting handbook. Illuminating Engineering, 2000.
[37] CIE Commission Internationale de l'Éclairage. Proceedings, Light as a true visual quantity: Principles of measurement. CIE 041, 1978.
[38] Rea MS, Bullough JD, Freyssinier-Nova JP, Bierman A. A proposed unified system of photometry. Lighting Res Technol 2004;36:85–109.
[39] Eloholma M, Viikari M, Halonen L, Walkey H, Goodman T, Alferdinck J, Freiding A, Bodrogi P, Várady G. Mesopic models – from brightness matching to visual performance in night-time driving: a review. Lighting Res Technol 2005;37:155–73.
[40] Goodman T, Forbes A, Walkey H, Eloholma M, Halonen L, Alferdinck J, Freiding A, Bodrogi P, Várady G, Szalmas A. Mesopic visual efficiency IV: A model with relevance to nighttime driving and other applications. Lighting Res Technol 2007;39:365–92.
[41] CIE Commission Internationale de l'Éclairage. Technical Report 191: 2010 – Recommended system for mesopic photometry based on visual performance, 2010.
[42] Rea MS, Figueiro MG, Bierman A, Bullough JD. Circadian light. J Circadian Rhythms 2010;8:2. Available at: http://www.jcircadianrhythms.com/content/pdf/1740-3391-8-2.pdf.
[43] Gall D. Die Messung circadianer Strahlungsgrößen. Proceedings of 3. Internationales Forum fur den lichttechnischen Nachswuchs, Technische Universität Illmenau, 2004.
[44] Rea MS, Figueiro MG, Bierman A, Hamner R. Modeling the spectral sensitivity of the human circadian system. Lighting Res Technol 2011;43:1–12.
[45] Figueiro MG, Rea MS. Lack of short-wavelength light during the school day delays dim light melatonin onset (DLMO) in middle school students. Neuro Endocrinol Lett 2010;31:92–6.
[46] Berman SM. Energy efficiency consequences of scotopic sensitivity. J Illumin Eng Soc 1992;21:3–14.
[47] Berman SM, Navvab M, Martin MJ, Sheedy J, Tithof W. A comparison of traditional and high colour temperature lighting on the near acuity of elementary school children. Lighting Res Technol 2006;38:41–9.
[48] Koole R. Fundamentals and applications of semiconductor nanocrystals: a study on the synthesis, optical properties, and interactions of quantum dots. PhD Thesis, Netherlands: Utrecht University; 2008.
[49] Bera D, Qian L, Holloway PH. Semiconducting quantum dots for bioimaging. In: Pathak Y, Thassu D, editors. Drug delivery nanoparticles formulation and characterization. London, UK: Informa Healthcare; 2009:349–66.
[50] Gaponik N, Hickey SG, Dorfs D, Rogach AL, Eychmüller A. Progress in the light emission of colloidal semiconductor nanocrystals. Small 2010;6:1364–78.
[51] Greytak AB, Allen PM, Liu W, Zhao J, Young ER, Popović Z, Walker BJ, Nocera DG, Bawendi MG. Alternating layer addition approach to CdSe/CdS core/shell quantum dots with near-unity quantum yield and high on-time fractions. Chem Sci 2012;3:2028–34.
[52] Jain PK, Beberwyck BJ, Fong L-K, Polking MJ, Alivisatos AP. Highly luminescent nanocrystals from removal of impurity atoms residual from ion-exchange synthesis. Angew Chem Int Ed 2012;51:2387–90.
[53] Reiss P, Protière M, Li L. Core/shell semiconductor nanocrystals. Small 2009;5:154–68.
[54] Wang X, Yan X, Li W, Sun K. Doped quantum dots for white-light-emitting diodes without reabsorption of multiphase phosphors. Adv Mater 2012;24:2742–7.
[55] Demir HV, Nizamoglu S, Erdem T, Mutlugun E, Gaponik N, Eychmüller A. Quantum dot integrated LEDs using photonic and excitonic color conversion. Nano Today 2011;6:632–47.
[56] American National Standard for Electric Lamps – Specifications for the Chromaticity of Solid State Lighting (SSL) Products, 2008.
[57] Erdem T, Demir HV. Efficient LED road lighting with high color rendering using quantum dot nanophosphors (submitted).
[58] British Standard BS 5489-1:2003 – Code of practice for the design of road lighting, 2003.
[59] IESNA Illuminating Engineering Society of North America, Recommended Practice RP-8-00 Roadway lighting, 2005.
[60] Achermann M, Petruska MA, Koleske DD, Crawford MH, Klimov VI. Nanocrystal-based light-emitting diodes utilizing high-efficiency nonradiative energy transfer for color conversion. Nano Lett 2006;6:1396–00.
[61] Chen H-S, Hsu C-K, Hong H-Y. InGaN-CdSe-ZnSe quantum dots white LEDs. IEEE Photonic Tech L 2006;18:193–5.
[62] Chen H-S, Yeh D-M, Lu C-F, Huang C-F, Shiao W-Y, Huang J-J, Yang CC, Liu I-S, Su W-F. White light generation with CdSe-ZnS nanocrystals coated on an InGaN-GaN quantum-well blue/Green two-wavelength light-emitting diode. IEEE Photonic Tech L 2006;18:1430–2.
[63] Nizamoglu S, Ozel T, Sari E, Demir HV. White light generation using CdSe/ZnS core-shell nanocrystals hybridized with InGaN/GaN light emitting diodes. Nanotechnology 2007;18:065709.
[64] Nizamoglu S, Zengin G, Demir HV. Color-converting combinations of nanocrystal emitters for warm-white light generation with high color rendering index. Appl Phys Lett 2008;92:031102–031102-3.
[65] Nizamoglu S, Erdem T, Sun XW, Demir HV. Warm-white light-emitting diodes integrated with colloidal quantum dots for high luminous efficacy and color rendering. Opt Lett 2010;35:3372–4.
[66] Nizamoglu S, Erdem T, Demir HV. High scotopic/photopic ratio white-light-emitting diodes integrated with semiconductor nanophosphors of colloidal quantum dots. Opt Lett 2011;36:1893–5.
[67] Nizamoglu S, Mutlugun E, Özel T, Demir HV, Sapra S, Gaponik N, Eychmüller A. Dual-color emitting quantum-dot-quantum-

well CdSe-ZnS heteronanocrystals hybridized on InGaN/GaN light emitting diodes for high-quality white light generation. Appl Phys Lett 2008;92:113110.
[68] Wang X, Li W, Sun K. Stable efficient CdSe/CdS/ZnS core/multi-shell nanophosphors fabricated through a phosphine-free route for white light-emitting-diodes with high color rendering properties. J Mater Chem 2011;21:8558.
[69] Song W-S, Yang H. Efficient white-light-emitting diodes fabricated from highly fluorescent copper indium sulfide core/shell quantum dots. Chem Mater 2012;24:1961–7.
[70] Song W-S, Yang H. Fabrication of white light-emitting diodes based on solvothermally synthesized copper indium sulfide quantum dots as color converters. Appl Phys Lett 2012;100:183104.
[71] Mutlugun E, Hernandez-Martinez PL, Eroglu C, Coskun Y, Erdem T, Sharma VK, Unal E, Panda SK, Hickey SG, Gaponik N, Eychmüller A, Demir HV. Large-area (over 50 cm×50 cm) Freestanding films of colloidal InP/ZnS quantum dots. Nano Lett 2012;12:3986–93.
[72] Kim S, Kim T, Kang M, Kwak SK, Yoo TW, Park LS, Yang I, Hwang S, Lee JE, Kim S-K, Kim S-W. Highly luminescent InP/GaP/ZnS nanocrystals and their application to white light-emitting diodes. J Am Chem Soc 2012;134:3804–9.
[73] Woo JY, Kim K, Jeong S, Han C-S. Enhanced photoluminance of layered quantum dot – phosphor nanocomposites as converting materials for light emitting diodes. J Phys Chem C 2011;115:20945–52.
[74] Kundu J, Ghosh Y, Dennis AM, Htoon H, Hollingsworth JA. Giant nanocrystal quantum dots: stable down-conversion phosphors that exploit a large stokes shift and efficient shell-to-core energy relaxation. Nano Lett 2012;12:3031–7.
[75] Nizamoglu S, Mutlugun E, Akyuz O, Kosku Perkgoz N, Demir HV, Liebscher L, Sapra S, Gaponik N, Eychmüller A. White emitting CdS quantum dot nanoluminophores hybridized on near-ultraviolet LEDs for high-quality white light generation and tuning. New J Phys 2008;10:023026.
[76] Chandramohan S, Ryu BD, Kim HK, Hong C-H, Suh E-K. Trap-state-assisted white light emission from a CdSe nanocrystal integrated hybrid light-emitting diode. Opt Lett 2011;36:802–4.
[77] Gosnell JD, Schreuder MA, Rosenthal SJ, Weissa SM. Efficiency improvements of white-light CdSe nanocrystal-based LEDs. Proc SPIE 2007;66690R.
[78] Nizamoglu S, Demir HV. Hybrid white light sources based on layer-by-layer assembly of nanocrystals on near-UV emitting diodes. Nanotechnology 2007;18:405702.
[79] Ziegler J, Xu S, Kucur E, Meister F, Batentschuk M, Gindele F, Nann T. Silica-coated InP/ZnS nanocrystals as converter material in white LEDs. Adv Mater 2008;20:4068–73.
[80] Changyu S. CdSe/ZnS/CdS core/shell quantum dots for white LEDs. Proc SPIE 2008;7138:71382E.
[81] Kim JU, Lee MH, Yang H. Synthesis of $Zn_{(1-x)}Cd_{(x)}S$:Mn/ZnS quantum dots and their application to light-emitting diodes. Nanotechnology 2008;19:465605.
[82] Wang H, Lee KS, Ryu JH, Hong CH, Cho YH. White light emitting diodes realized by using an active packaging method with CdSe/ZnS quantum dots dispersed in photosensitive epoxy resins. Nanotechnology 2008;19:145202.
[83] Jang HS, Heesun Yang H, Kim SW, Han JY, Lee S-G, Jeon DY. White light-emitting diodes with excellent color rendering based on organically capped CdSe quantum dots and Sr_3SiO_5:Ce^{3+}, Li^+ phosphors. Adv Mater 2008;20:2696–702.
[84] Jang HS, Kwon B-H, Yang H, Jeon DY. Bright three-band white light generated from CdSe/ZnSe quantum dot-assisted Sr_3SiO_5:Ce^{3+}, Li^+-based whitelight-emitting diode with high color rendering index. Appl Phys Lett 2009;95:161901.
[85] Huang C-Y, Su Y-K, Chuang RW, Chen Y-C, Huang T-S, Wan C-T. Tetrachromatic hybrid white light-emitting diodes and the energy transfer between conjugated polymers and CdSe/ZnS quantum dots. J Electrochem Soc 2009;156:H625–8.
[86] Yu HJ, Park K, Chung W, Kim J, Kim SH. White light emission from blue InGaN LED precoated with conjugated copolymer/quantum dots as hybrid phosphor. Synthetic Metals 2009;159:2474–7.
[87] Cheng G, Mazzeo M, Rizzo A, Li Y, Duan Y, Gigli G. White light-emitting devices based on the combined emission from red CdSe/ZnS quantum dots, green phosphorescent, and blue fluorescent organic molecules. Appl Phys Lett 2009;94:243506.
[88] Song W-S, Kim H-J, Kim Y-S, Yang H. Synthesis of $Ba_2Si_3O_8$:Eu^{2+} phosphor for fabrication of white light-Emitting diodes assisted by ZnCdSe/ZnSe quantum dot. J Electrochem Soc 2010;157:J319–23.
[89] Woo JY, Kim KN, Jeong S, Han CS. Thermal behavior of a quantum dot nanocomposite as a color converting material and its application to white LED. Nanotechnology 2010;21:495704.
[90] Changyu S. White LED based on YAG: Ce, Gd phosphor and CdSe-ZnS core/shell quantum dots. Proc SPIE 2008;7138:71382E.
[91] Gosnell JD, Rosenthal SJ, Weiss SM. White light emission characteristics of polymer-encapsulated CdSe nanocrystal films. IEEE Photon Technol Lett 2010;22:541–3.
[92] Dai J, Ji Y, Xu CX, Sun XW, Leck KS, Ju ZG. White light emission from CdTe quantum dots decorated n-ZnO nanorods/p-GaN light-emitting diodes. Appl Phys Lett 2011;99:063112.
[93] Jung H, Chung W, Lee CH, Kim SH. Fabrication of white light-emitting diodes based on UV light-emitting diodes with conjugated polymers-(CdSe/ZnS) quantum dots as hybrid phosphors. J Nanosci Nanotechnol 2012:12:5407–11.
[94] Shen C, Chu J, Qian F, Zou X, Zhong C, Li K, Jin S. High color rendering index white LED based on nano-YAG:Ce^{3+} phosphor hybrid with CdSe/CdS/ZnS core/shell/shell quantum dots. J Mod Opt 2012;59:1199–203.
[95] Zhu L, Xu L, Wang J, Yang S, Wang C-F, Chen L, Chen S. Macromonomer-induced CdTe quantum dots toward multicolor fluorescent patterns and white LEDs. RSC Advances 2012;2:9005–10.
[96] Song W-S, Kim J-H, Lee J-H, Lee H-S, Do YR, Yang H. Synthesis of color-tunable Cu-In-Ga-S solid solution quantum dots with high quantum yields for application to white light-emitting diodes. J Mater Chem 2012;22:21901–8.
[97] Wikipedia contributors CIE 1931 color space. Wikipedia, the free encyclopedia, 2012. (Accessed Sep 5, 2012 at http://en.wikipedia.org/w/index.php?title=CIE_1931_color_space&oldid=509071050).
[98] Kim T-H, Cho K-S, Lee EK, Lee SJ, Chae J, Kim JW, Kim DW, Kwon J-Y, Amaratunga G, Lee SY, Choi BL, Kuk Y, Kim JM, Kim K. Full-colour quantum dot displays fabricated by transfer printing. Nat Photonics 2011;5:176–82.
[99] Chen K-J, Chen H-C, Tsai K-A, Lin C-C, Tsai H-H, Chien S-H, Cheng B-S, Hsu Y-J, Shih M-H, Tsai C-H, Shih H-H, Kuo H-C. Resonant-enhanced full-color emission of quantum-dot-based display technology using a pulsed spray method. Adv Funct Mater 2012; 22:5138–43.